A strategy to suppress STAT1 signalling conserved in pathogenic poxviruses and paramyxoviruses

Callum Talbot-Cooper[1], Teodors Pantelejevs[2], John P. Shannon[1,3], Christian R. Cherry[3], Marcus T. Au[1], Marko Hyvönen[2], Heather D. Hickman[3] and Geoffrey L. Smith[1*]

[1] Department of Pathology, University of Cambridge, Tennis Court Road, Cambridge, CB2 1QP

[2] Department of Biochemistry, University of Cambridge, 80 Tennis Court Road, Cambridge, CB2 1GA

[3] Viral Immunity and Pathogenesis Unit, Laboratory of Clinical Immunology and Microbiology, National Institute of Allergy and Infectious Diseases, National Institutes of Health, Bethesda, Maryland 20852, USA

* Corresponding Author: gls37@cam.ac.uk (GLS)

Summary

The induction of interferon-stimulated genes by signal transducer and activator of transcription (STAT) proteins, is a critical host defence to fight virus infections. Here, a highly expressed poxvirus protein 018 is shown to inhibit IFN-induced signalling by binding the SH2 domain of STAT1 to prevent STAT1 association with an activated IFN receptor. Despite the presence of additional inhibitors of IFN-induced signalling, a poxvirus lacking 018 was attenuated in mice. The 2.0 Å crystal structure of the 018:STAT1 complex reveals a mechanism for a high-affinity, pTyr-independent mode of binding to an SH2 domain. Furthermore, the STAT1 binding motif of 018 shows sequence similarity to the STAT1-binding proteins from Nipah virus, which like 018, block the association of STAT1 with an IFN receptor. Taken together, these results provide detailed mechanistic insight into a potent mode of STAT1 antagonism, found to exist in genetically diverse virus families.

Introduction

Interferons (IFNs) activate signal transduction pathways to upregulate IFN-stimulated genes (ISGs) that inhibit virus replication and spread (Schneider et al., 2014). Signal transduction is mediated by signal transducers of transcription (STAT) proteins STAT1 and STAT2, which, in an unstimulated state, exist as latent unphosphorylated hetero (U-STAT1-U-STAT2) or homodimers (U-STAT1) (Mao et al., 2005; Wang et al., 2021). IFNs bind their cognate receptors to activate receptor-associated kinases that in turn phosphorylate receptor tails creating a docking site for STAT SH2 domains. At the receptors, STATs are phosphorylated (pSTAT) and undergo dimer rearrangement from an anti-parallel to an activated parallel conformation, mediated by a reciprocal pTyr:SH2 interaction between two pSTATs (Wenta et al., 2008).

Type I IFNs (IFN-I) signal through the IFNα/β receptor (IFNAR) to activate kinases that phosphorylate STAT1 and 2. The pSTAT1:STAT2 heterodimer associates with IRF9 to form a trimeric complex known as IFN-stimulated gene factor 3 (ISGF3) (Rengachari et al., 2018). Type II IFN (IFN-II), of which IFNγ is the sole member, signals through the IFNγ receptor (IFNGR) and activates kinases that phosphorylate STAT1 only. The pSTAT1 homodimer is known as the gamma-activated factor (GAF). Nuclear ISGF3 and GAF drive the transcription of ISGs with IFN-stimulated responsive element (ISRE) or gamma-activated sequence (GAS) promoters, respectively (Aaronson and Horvath, 2002).

To overcome the anti-viral activities induced by IFNs, viruses have evolved numerous strategies to antagonise host IFN-pathways, for reviews see (García-Sastre, 2017; Randall and Goodbourn, 2008). Given the importance of viral-mediated IFN-signalling antagonism for

51 productive infection, mechanistic insight into these strategies can guide novel anti-viral
52 therapeutic approaches.
53
54 Poxviruses are large, cytoplasmic DNA viruses. Vaccinia virus (VACV) is the prototypic
55 poxvirus, the vaccine used to eradicate smallpox and an excellent model to study host-pathogen
56 interactions. VACV encodes about 200 proteins of which it is estimated that >1/3 modulate
57 host immune responses, including proteins that target IFN-induced signalling pathways (Smith
58 et al., 2013, 2018). VACV proteins B18 and B8 act as soluble IFN receptors that bind IFN-I
59 and IFN-II, respectively (Alcamí and Smith, 1995; Colamonici et al., 1995; Mossman et al.,
60 1995; Symons et al., 1995). At the intracellular level, the viral phosphatase vH1
61 dephosphorylates STAT1 (Koksal et al., 2009; Najarro et al., 2001), whilst protein C6 inhibits
62 IFN-I signalling in the nucleus (Stuart et al., 2016).
63
64 Here we show that an uncharacterised viral protein (018), encoded by gene VACWR018 of
65 VACV strain Western Reserve (WR), binds directly to the SH2 domain of STAT1 and
66 competes with a phosphorylated IFN receptor to prevent STAT1 receptor association and
67 subsequent STAT1 phosphorylation. A VACV lacking 018 was attenuated in mice and induced
68 enhanced innate immune signalling, demonstrating the *in vivo* importance of this inhibitor of
69 IFN-induced signalling for poxviruses. The crystal structure of 018 complexed with STAT1
70 was determined to 2.0 Å. This revealed a key contact that enables 018 to bind STAT1 and
71 STAT4 selectively, and a non-canonical SH2 binding mode, whereby 018 occupies the SH2
72 domain in a pTyr pocket-independent manner with high affinity. The 018 STAT1-binding
73 motif is identical in variola virus and monkeypox virus orthologues of 018. In addition, it shares
74 remarkable similarity to STAT1-binding regions of V/W and P proteins from Nipah virus
75 (NiV), a highly pathogenic paramyxovirus. Like 018, we show that the minimal STAT1

76 binding region of NiV-V protein can compete with a phosphorylated IFN receptor to bind
77 STAT1. This study reveals a conserved mechanism for targeting STAT1 utilised by members
78 of the poxvirus and paramyxovirus families, to subvert cellular anti-viral responses.

Results

The 018 open reading frame (ORF) from VACV WR (gene VACWR018) is transcribed early during infection and is one of the most abundant viral transcripts (Assarsson et al., 2008; Wennier et al., 2013; Yang et al., 2015). Protein 018 is highly conserved within the orthopoxvirus genus including human pathogens cowpox virus, monkeypox virus and variola virus, the causative agent of smallpox (**Figure** S1). The 018 ORF is also highly conserved in ancient variola viruses dating from the Viking age (Mühlemann et al., 2020).

As 018 is expressed early during infection, is highly abundant, and encoded within a region of the genome known to harbour immunomodulators (Gubser et al., 2004), we explored if 018 modulates anti-viral immunity.

Vaccinia protein 018 inhibits IFN-induced signalling

To test if 018 modulates anti-viral immunity, reporter plasmids were used that express a luciferase (Luc) gene upon activation of specific anti-viral signalling pathways. Activation of IRF3, NF-kB and AP-1 pathways that induce IFNs (specifically IFNβ) were measured using an IFNβ-Luc reporter after stimulation with Sendai virus (SeV), the prototypic paramyxovirus. Downstream, IFN-induced pathways were measured using ISRE or GAS-Luc reporters after stimulation with IFN-I (IFNα) or IFN-II (IFNγ), respectively.

TAP-tagged (2 X Strep, 1 X FLAG epitope) 018 inhibited pathway activation induced by IFN-I and II (**Figure 1A, B**), whereas it had little effect on the activation of IFNβ-Luc (**Figure 1C**).

NiV-V (Rodriguez et al., 2002) and VACV protein C6 (Stuart et al., 2016; Unterholzner et al., 2011) were used as positive controls, whereas VACV protein N1 (Maluquer de Motes et al., 2011) was used as a negative control.

Next, the effect of 018 on expression of endogenous ISGs was tested. T-REx 293 cell lines that inducibly expressed TAP-tagged 018 or controls (EV, TAP-tagged N1 or NiV-V) were stimulated with IFN-I or -II and representative ISGs were analysed by immunoblotting. Stimulation with IFN led to an increase in ISG levels in cells expressing either EV, or N1 (**Figure 1D, E**). In contrast, 018 blocked upregulation of ISGs after stimulation with either IFN-I or IFN-II **(Figure 1D, E**). These data show 018 is a potent inhibitor of IFN-I and -II-induced signalling.

Phosphorylation of STAT1 at Tyr 701 is blocked by 018

To assess if 018 inhibited STAT translocation into the nucleus, HeLa cells were transfected with TAP-tagged 018 or controls and then stimulated with IFN-I or -II. In untransfected cells, stimulation with IFN-I or -II induced STAT1 redistribution to the nucleus (**Figure 2A**), whereas only IFN-I did so for STAT2 (**Figure 2B**). In contrast, translocation of STAT1 and 2 was blocked in cells expressing 018 (**Figure 2A, B)**. Consistent with previous reports, NiV-V also blocked STAT1 translocation, but unlike 018, NiV-V redistributed STAT1 to a predominantly cytoplasmic localisation in non-stimulated cells due to harbouring a nuclear export signal (Rodriguez et al., 2004) (**Figure 2A**).

Prior to translocation, STATs are phosphorylated at conserved tyrosine residues near their C terminus. To test if 018 inhibited phosphorylation of STAT1 at Tyr701 (pSTAT1) and STAT2 at Tyr-690 (pSTAT2), T-REx 293 cells expressing TAP-tagged 018 or controls were stimulated with IFN-I or -II and lysates were analysed by immunoblotting. IFN-I stimulation increased pSTAT1 and pSTAT2 levels in both EV and N1-expressing cells, whereas cells expressing 018 showed very low levels of pSTAT1 (**Figure 2C, Figure S2A**). In contrast, 018 only affected pSTAT2 levels marginally (**Figure 2C, Figure S2B**). Consistent with previous reports, NiV-V blocked STAT1 phosphorylation (Rodriguez et al., 2002). Interestingly, NiV-V also blocked STAT2 phosphorylation, which has not been reported previously, but is consistent with NiV-V harbouring a distinct STAT2-binding site (Rodriguez et al., 2004). IFN-II increased pSTAT1 in control cells, whereas STAT1 phosphorylation was blocked by 018 (and NiV-V) (**Figure 2D, Figure S2C**). These data show 018 blocks phosphorylation of STAT1 at Tyr701 after stimulation with IFN-I or -II and thus prevents STAT1/2 translocation.

A minimal 21 aa fragment of 018 is sufficient to bind STAT1

Next, we assessed if 018 interacts with cellular proteins involved in IFN signal transduction. TAP-tagged 018 was expressed in 2fTGH cells and its ability to co-precipitate STAT1, STAT2 and IRF9 was assessed by pulldown. 018 co-precipitated STAT1 and to a lesser degree STAT2, whereas no interaction with IRF9 was observed (**Figure 3A**). In 2fTGH-derived STAT1 knockout cells (U3A), the 018:STAT2 interaction was lost, indicating the interaction was either indirect via STAT1, or STAT1 was required for 018 to precipitate STAT2 (**Figure 3B**). In 2fTGH-derived STAT2 knockout cells (U6A), the 018:STAT1 interaction was retained (**Figure 3B**). The 018:STAT1 interaction was confirmed to be direct as 018 and STAT1 still

co-precipitated when expressed by a cell-free based transcription and translation system (**Figure S3A**).

To characterise the 018:STAT1 interaction, each protein was expressed and purified from *E. coli*. 018 was fused to the B1 domain of protein G (GB1) to improve solubility and expression. Using isothermal titration calorimetry (ITC), we observed a K_D value of 291 nM, with a stoichiometry of 1.02, indicating a single 018 molecule binds per U-STAT1 protomer (**Figure 3C**). The effect of 018 on U-STAT1 quaternary assembly was evaluated by SEC-MALS. U-STAT1 alone eluted predominantly as tetrameric and dimeric species, and preincubation with excess GB1-018 resulted in the two peaks having earlier elution volumes and increased masses (**Figure S3B**). This indicates that 018 binds U-STAT1 without altering its oligomeric state.

Next, the region of 018 required to inhibit IFN signalling was mapped. C-terminal and N-terminal truncations of 018 were constructed and their ability to inhibit IFN-I and -II signalling was assessed (**Figure 3D-F**). For ease of interpretation, inhibitory activity was categorised as (i) greater than 95%, (ii) between 75% and 95%, or (iii) less than 25%, which was deemed to be non-inhibitory. Mutant 1-35 had the largest C-terminal truncation and still demonstrated >95% inhibition (**Figure 3E,F**). Mutant 8-60 inhibited >95%, whereas mutant 22-60 lost inhibitory activity (<25%) and showed comparable expression to the full-length protein (**Figure 3E,F**). These data show that aa 8-35 of 018 is sufficient for pathway inhibition.

To refine the region of 018 responsible for pathway inhibition, additional mutants, truncating inwards from aa 8 and 35 were constructed (**Figure S3C**). Mutant 11-60 retained >95% inhibition whereas mutants with further N-terminal truncation had reduced inhibitory activity despite WT expression levels (**Figure S3D,E**). Mutant 1-30 inhibited between 75%-95%,

174 demonstrating a marginal loss in inhibitory activity, however, expression was undetectable
175 (**Figure S3D,E**). All further C-terminal truncations showed <25% inhibitory activity, but
176 again, expression was undetectable (**Figure S3D,E**). The same pattern of inhibitory activity by
177 018 truncations mutants was observed for both IFN-I and -II signalling (**Figure S3F**),
178 indicating the same region of 018 is required to inhibit both pathways.
179
180 These observations map a putative minimal inhibitory region of 018 to aa 11-31. The C-
181 terminal boundary was defined assuming the slight reduction in inhibitory activity after
182 deletion of residues 35-31 was due to lower protein expression levels, whereas further
183 truncation removed functional residues. Ser31 is included within the minimal inhibitory region
184 as it is highly conserved in orthopoxvirus orthologues of 018 (**Figure S1)**.
185
186 ITC measurements of the putative minimal fragment (018^{T2}) with STAT1 gave a K_D of 235
187 nM, a value comparable to that of full length 018 (291 nM) (**Figure 3H)**. Removal of the C-
188 terminal 28-TYTS-31 (018^{T3}) from the putative minimal fragment led to a large reduction in
189 affinity (>10 μM), thereby demonstrating the importance of these residues (**Figure 3I)**.
190 Collectively, these data show that a 21-residue segment of 018, aa 11-31, is sufficient for
191 maximal STAT1 binding and inhibitory activity.
192

193 **018 is a virulence factor**

194 To study the role of 018 during infection, a VACV (strain WR) 018 deletion mutant (termed
195 vΔ018) was constructed. The wild-type sibling virus (termed v018) and vΔ018 were analysed
196 by PCR (**Figure S4A**) and genomic sequencing, which showed no differences other than the
197 intended deletion of the 018 ORF. Comparison of v018 and vΔ018 in cell culture displayed no

198 difference in replication or plaque size (**Figure S4B-D**). Another VACV (termed vTAP-018)
199 was constructed by reintroduction of the 018 ORF fused to an N-terminal TAP-tag into vΔ018
200 at its natural locus. Pulldown of TAP-tagged 018 expressed from vTAP-018 confirmed the
201 018:STAT1 interaction during infection (**Figure S4E, F**).
202
203 Next, vΔ018's ability to inhibit IFN signalling was assessed. A549 cells were infected with
204 v018 or vΔ018 and, at the indicated times p.i., were stimulated with either IFN-I or -II, after
205 which the pSTAT1 level was determined by immunoblotting. Cells were washed once prior to
206 stimulation to remove the majority of soluble VACV IFN decoy receptors B8 and B18. This,
207 however, will not fully remove B18 (IFN-I decoy receptor) due to its ability to bind to the cell
208 surface (Alcamí et al., 2000). Although by 2 h p.i., both v018 and vΔ018 inhibited pSTAT1
209 induction after IFN-I stimulation, v018 inhibited earlier and to a greater extent. **(Figure 4A)**.
210 In contrast, pSTAT1 induction was inhibited by v018 but almost fully rescued to mock levels
211 in vΔ018-infected cells after IFN-II stimulation **(Figure 4B)**. Consistent with this finding,
212 STAT1 translocation was blocked by v018 after IFN–II stimulation, whereas in vΔ018-infected
213 cells, STAT1 was predominantly nuclear **(Figure 4C)**. The impaired ability of vΔ018 to inhibit
214 IFN-II signalling was illustrated further by increased IRF1 levels (a canonical IFNγ ISG) in
215 cells infected with v018 compared to vΔ018 after IFN-II stimulation at both the mRNA
216 (**Figure S4G**) and protein level (**Figure 4D**).
217
218 To evaluate if 018 contributes to virulence, BALB/c mice were infected via the intranasal route
219 with either v018 or vΔ018 and their weight was measured daily (**Figure 4E)**. Mice infected
220 with vΔ018 lost significantly less weight than those infected with v018 (**Figure 4E)** and
221 showed reduced virus titres at 7 and 9 days p.i. (**Figure 4F**). Furthermore, consistent with 018

functioning as an immunomodulator, mRNAs for several ISGs, chemokines and IFNs were upregulated in the lungs of mice infected with vΔ018 compared to v018 (**Figure 4G)**. Collectively, these data show VACV lacking 018 is defective in inhibition of IFN-induced signalling and is attenuated in mice.

018 binds the STAT1 SH2 domain to block its association with the phosphorylated IFNGR1

To identify which STAT1 domain/s 018 binds, the ability of 018 to interact with several STAT1 truncations and STAT1-STAT3 chimeras was tested (**Figure 5A**). 018 bound a chimera with linker domain (LD), SH2 and transactivation domain (TAD) of STAT1 (31F), but not a chimera with coiled-coil and DNA-binding domains of STAT1 (13F) (**Figure 5B**). These chimeras have been studied with NiV-V, which also only binds 31F (Rodriguez et al., 2004). 018 bound STAT1 C-terminal truncations that lack the final 38 residues (STAT1β, a naturally occurring isoform of STAT1) or the entire TAD (**Figure 5C**). Lastly, 018 bound a chimera that contained only the SH2 and TAD of STAT1 (Fus 1) but not a chimera that contained the LD of STAT1 (Fus 2) nor with STAT3 alone (**Figure 5D**). Together, these pulldowns show 018 binds the SH2 domain of STAT1.

The finding that 018 binds the SH2 domain allowed us to hypothesise how 018 blocks STAT1 phosphorylation. Given that 018 inhibition of IFN-II signalling during infection was non-redundant, we focused on this pathway to study 018 mechanistically. The IFNGR is composed of two ligand-binding IFNGR1 chains and two IFNGR2 chains and binds dimeric IFNγ (Mendoza et al., 2019). Ligand engagement induces JAK-1 phosphorylation of IFNGR1 at

Tyr440 (Briscoe et al., 1996; Greenlund et al., 1994). STAT1 then docks at the IFNGR1 pTyr site via its SH2 domain and is itself phosphorylated (Greenlund et al., 1995). pSTAT1 then undergoes structural rearrangement to a parallel dimer orientation and dissociates from the receptor. We hypothesised that by binding the SH2 domain, 018 blocks STAT1 recruitment to pIFNGR1 and thus prevents STAT1 phosphorylation.

To test this, a fluorescence polarisation (FP) assay was established using a fluorescent 12-mer peptide corresponding to the pIFNGR1 sequence harbouring the STAT1 docking site (pYDKPH) as a probe. Addition of 018 to a preformed STAT1-pIFNGR1 probe led to a dose-dependent displacement of probe and an IC_{50} value of 1.26 μM (**Figure 5E**). IC_{50} values of 0.93 μM and 17.82 μM for 018^{T2} and 018^{T3}, respectively, were obtained, demonstrating that 018^{T2}, but not 018^{T3}, has comparable inhibitory activity to full length 018, consistent with ITC data (**Figure 5E**).

The mechanism was further validated by competition ITC. A 5-mer peptide corresponding to the pIFNGR1 docking region (pYDKPH) was titrated into U-STAT1, giving a K_D value of 7.6 μM (**Figure 5F**). In contrast, inclusion of excess 018 in the calorimeter cell resulted in complete loss of detectable binding (**Figure 5G**). Taken together, these data demonstrate a competitive inhibition mechanism, whereby 018 binds the SH2 of STAT1 and prevents STAT1 from engaging the active IFN signalling receptor complex.

Vaccinia 018 and Nipah virus V protein utilise a shared motif to engage STAT1

NiV-V, W and P proteins, encoded by the P gene, all inhibit IFN signalling. They have distinct C-terminal sequences but share a common 407 aa N-terminal region to which the IFN inhibitory activity was mapped (aa 114-140) (Ciancanelli et al., 2009). Here, we focus on this STAT1-binding region and refer to this within NiV-V.

The observation that 018 and NiV-V bind STAT1, block STAT1 phosphorylation and bind the 31F chimera suggested they might share a similar mode of action. Alignment of the NiV-V STAT1 binding region and 018^{T2} revealed aa similarity exemplified by a conserved HxH motif preceded by a cluster of conserved hydrophobic residues (**Figure 6A**). Recent ITC data showed a NiV-V fragment (aa 92-190) binds STAT1 directly but weakly (K_D >100 μM) and mutation of 117-HDH-119 to 117-AAA-119 abolished binding (Jensen et al., 2020). To determine whether the HxH motif of 018 had analogous function, we mutated 17-HGH-19 to 17-AGA-19 (018^{AGA}). Unlike 018, 018^{AGA} did not co-precipitate with endogenous STAT1 in cells (**Figure S5**). Furthermore, ITC titration of purified GB1-fused 018^{AGA} into STAT1 resulted in no detectable binding (**Figure 6B**). Loss in STAT1 binding ability correlated with a loss of inhibitory activity because 018^{AGA} was unable to inhibit IFN-I and -II signalling by reporter gene assay (**Figure 6C,D**). Consistent with this, 018^{AGA} did not interfere with STAT1:pIFNGR1 12-mer interaction by FP (**Figure 6G**). In addition, 018^{AGA} showed no inhibition of STAT1-pIFNGR1 binding via ITC (**Figure 6H**).

Consistent with the idea that 018 and NiV-V harbour analogous motifs, recently the site for NiV-V binding to STAT1 was mapped to the SH2 domain of STAT1 (Keiffer et al., 2020). To assess if these viral proteins target the same SH2 interface, the ability of 018 to outcompete the NiV-V:STAT1 interaction was tested. In cells transfected with TAP-tagged NiV-V, NiV-V co-precipitated with endogenous STAT1, however, this was decreased in a dose-dependent

manner by expression of HA-tagged 018 (**Figure 6E**). In contrast, HA-tagged 018^{AGA} did not affect the NiV-V:STAT1 interaction (**Figure 6F**). These data show that 018 and NiV-V utilise a shared motif to bind a common interface on the SH2 domain of STAT1.

Previous reports show NiV-V sequesters STAT1 and 2 within the cytoplasm and prevents STAT1 phosphorylation (Rodriguez et al., 2002). The finding that 018 and NiV-V bind STAT1 via the same interface prompted us to assess if, like 018, NiV-V competes with pIFNGR1 to bind STAT1. To test this, NiV-V STAT1-binding fragment residues 110-140 ($NiV\text{-}V^{110\text{-}140}$) fused to a GB1 tag was purified together with a mutant in which His117 and His119 of the HxH motif were mutated to Ala ($NiV\text{-}V^{ADA}$). By FP assay, addition of NiV-V to the preformed STAT1-pIFNGR1 12-mer complex led to a modest reduction in polarisation, whereas addition of $NiV\text{-}V^{ADA}$ was non-competitive (**Figure 6I**). Consistent with these data, preincubation of STAT1 with NiV-V abolished any detectable binding between STAT1 and the pIFNGR 5-mer by ITC (**Figure 6J**). In contrast, preincubation with $NiV\text{-}V^{ADA}$ did not prevent STAT1:pIFNGR binding (**Figure 6K**). These data show that, in the context of IFN-II signalling, NiV-V can block STAT1 recruitment to the active IFNGR signalling complex.

Phosphotyrosine pocket-independent binding of 018 to the STAT1 SH2 domain

A feature of the SH2 interface is a deep pTyr pocket that binds the phosphate group and the phenyl ring of phosphotyrosine. Remarkably, 018 binds the STAT1 SH2 domain with high-affinity and competes with pIFNGR1 without a pTyr modification. Intrigued by this observation, we crystallised the STAT1 132-684 core fragment complexed with the minimal

018 peptide (Met11-Ser31). Crystals diffracted to 2.0 Å with 018 electron density clearly defined for most of the peptide, with only Ser31 not visible (**Figure S6A**).

The 018 peptide forms a β-hairpin fold with a β-turn midway through the sequence (**Figure 7A,B**) and the two strands of the peptide augment the central β-sheet of the SH2 domain, with Val14-His17 backbone hydrogen-bonding to the βD strand of the SH2 domain (**Figure 7C**). There is spatial overlap with published binding modes of pTyr peptides from pIFNGR1 and pSTAT1 homodimer (**Figure 7B**). The 680 $Å^2$ interface is formed by a large number of shallow contacts exclusively within the SH2 domain. Residues Trp12, Val14, Ile16 comprise a continuous hydrophobic interface with STAT1 helix αA and strand βD (**Figure 7D**). This is followed by a HxH motif, in which His17 forms an imidazole-to-imidazole hydrogen bond with His629 of STAT1 (**Figure 7D, E**). The His17 rotamer is stabilised intramolecularly by a second hydrogen bond with the backbone carbonyl of 018 Gly21. Gly18 carbonyl forms a hydrogen bond with Tyr651 hydroxyl of STAT1, similar to pIFNGR1 Pro443 (PDB: 1YVL). His19 occupies the same cleft as His444 of pIFNGR1, forming an identical π-stacking interaction with STAT1 Tyr634. The Asp20 sidechain stabilises the β-turn by hydrogen bonding with the Ser21 backbone and forms an intramolecular salt bridge with Lys24 (**Figure 7D**). An inter-strand hydrogen bond between the hydroxyl groups of Ser13 and Thr28 act as a non-covalent bridge that may stabilise the β-hairpin fold (**Figure 7D**).

Strikingly, 018 does not interact with the pTyr pocket. The only tyrosine in the peptide, Tyr29, hydrogen bonds with the ζ-amine of STAT1 Lys584 through its hydroxyl and makes van der Waals contacts with the alkyl chain of the same lysine (**Figure 7D**). The lower affinity of 018^{T3} compared to 018^{T2} may result from the loss of interactions made by Thr28 and Tyr29.

A single histidine found in STAT1 and 4 is a key determinant of 018 selectivity

High sequence similarity between SH2 domains of STATs led us to investigate if 018 interacts with other STATs. In humans, there are seven STATs (STAT1, 2, 3, 4, 5A, 5B and 6) (Ihle, 2001). U3A cells were co-transfected with V5-tagged STAT1-6 and TAP-tagged 018. Pulldown of 018 demonstrated that 018 binds STAT1 and STAT4, but not other STATs (**Figure 7F**).

To understand the observed specificity of 018 for STAT1 and 4, STAT SH2 domain alignments were integrated with our structural data (**Figure S6B**). In the crystal structure, a specific interaction between 018 His17 and His629 of STAT1 was observed. Only STAT1 and 4 have a histidine at this position, and so other STATs would fail to recapitulate this interaction. To test if STAT1 His629 was critical for specificity, a STAT3 mutant was made in which the structurally equivalent Glu635 was mutated to His. This enabled 018 to co-precipitate $STAT3^{Q635H}$, allowing the unambiguous assignment of specificity determinants of 018 binding (**Figure 7G**).

Discussion

STAT1 and 2 are central to IFN signalling and thus are common targets for viral antagonism (Harrison and Moseley, 2020), however structural details of STAT:antagonist complexes have remained elusive with a few exceptions. The complex of SeV C protein with the N-terminal domain of STAT1 indicates that C protein interferes with the oligomeric state of STAT1 (Oda et al., 2015) whilst the structures of dengue and Zika virus NS5 proteins in complex with STAT2 revealed that both NS5 proteins overlap the IRF9 binding site to prevent ISGF3

365 assembly (Wang et al., 2020). A similar mechanism was described for measles V protein
366 (Nagano et al., 2020). Here, the structure of 018, an uncharacterised poxvirus protein, with
367 STAT1, shows 018 occupies the STAT1 SH2 domain to block STAT1 association with the
368 active pIFNGR.
369
370 The molecular recognition between STAT SH2 domains and a pTyr site represents a conserved
371 mechanism for STAT recruitment to activated receptors. The pTyr is estimated to contribute
372 half the binding energy, while the remaining specificity is provided by a small number of
373 adjacent residues (Kaneko et al., 2010; Ladbury and Arold, 2011). For STAT1, 018 overlaps
374 with these specificity-determining sites and obstructs the pTyr pocket without occupying it.
375
376 To establish if a similar binding mode exists, we examined 524 SH2-containing structures
377 retrieved from PDB based on either Pfam or SMART annotation. The majority of liganded
378 SH2 domains bind a pTyr-containing peptide, a synthetic pTyr mimetic or an unphosphorylated
379 tyrosine at the pTyr pocket. Several structures contain SH2 domains as part of a larger protein-
380 protein interaction, in which the pTyr pocket is not occupied, however, in such cases, the
381 interface extends significantly beyond the SH2 phosphopeptide site. The closest binding mode
382 analogue to 018 was a monobody that binds at the phosphopeptide site of SHP-1 phosphatase
383 without interacting with the pTyr pocket itself (PDB: 6SM5). Hence, we suggest 018 has an
384 unprecedented mode of high-affinity SH2 domain binding.
385
386 For IFN-I-induced signalling, 018 blocked pSTAT1 induction but only modulated pSTAT2
387 levels minimally. After IFN-I stimulation, STAT2 docks at pTyr466 on IFNAR1 and
388 subsequently is phosphorylated at Tyr690 (Yan et al., 1996). The pTyr690 of STAT2 serves as
389 a docking site for STAT1 to present STAT1 for proximal phosphorylation at Tyr701 by JAKs

(Leung et al., 1995; Li et al., 1997; Qureshi et al., 1996). Additional Tyr phosphorylation sites on IFNAR2 are also important for ISGF3 formation and could serve as docking sites for STAT1 and 2 functioning in a cell type- or species-dependent manner (Zhao et al., 2008). Thus, we rationalise that during IFN-I signalling, occupancy of the STAT1 SH2 domain by 018 would diminish STAT1 engagement of either STAT2 pTyr690 or IFNAR to prevent STAT1 phosphorylation.

STAT4 was identified as an additional binding partner of 018. STAT4 is activated by phosphorylation predominantly in response to IL-12 and IFN-I and promotes IFNγ production during virus infection (Nguyen et al., 2002; Yang et al., 2020). The activation of STAT4 occurs mainly in lymphoid and myeloid cells, but also vascular endothelial cells (Torpey et al., 2004), thus, for 018 to modulate this pathway, VACV would need to infect these cell types *in vivo*. As the 018-binding interface is conserved between STAT1 and 4, functionally, 018 could prevent STAT4 recruitment to active receptors. Whether the 018:STAT4 interaction plays a physiological role during infection remains to be determined.

As STATs are an important class of drug targets in a wide range of diseases (Miklossy et al., 2013), the highly specific interaction of 018 for STAT1 and 4, notably via the HxH motif, presents a potential avenue for development of STAT1/4-selective inhibitors via rational drug design. One approach could involve the construction of peptidomimetic derivatives of the HxH motif in a structure-guided manner to deliver high-affinity binders.

The STAT1-binding region of 018 possesses significant sequence similarity to the STAT1-binding region of V/W and P proteins from NiV, a paramyxovirus first discovered in Malaysia in 1998 (Chua, 2000). NiV is highly pathogenic and has caused numerous sporadic outbreaks,

415 including recently in Kerala, India (Arunkumar et al., 2019) and no effective treatments or
416 vaccines are available (Hauser et al., 2021). Previous studies of NiV-V showed it sequesters
417 STAT1 and 2 and prevents STAT1 phosphorylation (Rodriguez et al., 2002). Our data advance
418 this observation and show that in the context of IFN-II signalling, the NiV STAT1 binding
419 region can block STAT1:pIFNGR1 association. Mechanistically, this is most relevant to the V
420 and P proteins due to their cytoplasmic location (Shaw et al., 2004). Although W harbours an
421 identical STAT1-binding region, it traffics STAT1 to the nucleus to prevent STAT1 activation
422 (Shaw et al., 2004). As we anticipate that the 114-VVYHDHGG-121 region of NiV-V/W and
423 P bind in an analogous fashion to the 14-VFIHGHDG-19 of 018, the 018:STAT1 structure can
424 aid understanding of previous mutagenesis studies of the NiV STAT1 binding region
425 (Ciancanelli et al., 2009; Hagmaier et al., 2006; Jensen et al., 2020; Ludlow et al., 2008;
426 Satterfield et al., 2019).
427
428 Intrinsically disordered proteins that harbour short linear motifs (SLiMs), such as the STAT1-
429 binding region from NiV and 018, are important mediators of virus-host interactions (Mishra
430 et al., 2020). SLiMs are advantageous to viruses because they offer high flexibility and
431 typically can evolve at fast rate allowing quick adaptation to changing host environments (Xue
432 et al., 2014). Virus SLiMs that mimic eukaryotic linear motifs have appeared as a prevalent
433 virus strategy to hijack cellular machinery and disable host defences (Davey et al., 2011; Hagai
434 et al., 2014; Lasso et al., 2021). Because SLiMs are short and evolve easily, they have emerged
435 predominantly independent of their host mimics rather than by horizontal gene transfer from
436 the host (Elde and Malik, 2009; Hagai et al., 2014). In the context of the 018/NiV-V STAT1-
437 binding motif, although it is possible cellular proteins do exist that bind STAT SH2 domains
438 in pTyr-independent manner, none have been identified and thus 018/NiV-V might not mimic
439 a cellular interaction. The STAT1-binding motif described here likely represents a striking

example of convergent evolution in diverse virus families and has produced an unconventional binding mechanism to target STAT1. Consistent with the notion that SLiMs preferentially target proteins central to multiple networks (Dyer et al., 2008), STAT1 is required for ISG induction in response to all IFN families (IFN-I, II and III). The existence of the shared motif between disparate viruses highlights its importance as an efficient moiety for inhibiting IFN-induced signalling.

It is notable that amongst the different STAT domains, the SH2 domain is the most highly conserved across various species (Park et al., 2008). Targeting this conserved domain may enable these viral antagonists to function in multiple species and contribute to the broad species specificity of VACV and NiV. Consistent with this notion, data presented here show that 018 antagonises human IFN signalling and contributes to VACV virulence in mice. Along the same lines, the VACV decoy IFN receptors B8 and B18 bind and neutralise IFNs from many species (Alcamí and Smith, 1995; Symons et al., 1995).

Poxviruses encode multiple antagonists of IFN-induced signalling. The earliest functioning of these, the viral phosphatase vH1, is carried within virions and released into the cytoplasm upon infection where it might dephosphorylate STAT1, although this activity has been demonstrated only in vitro (Najarro et al., 2001; Schmidt et al., 2013). Multiple reports have shown that shortly after VACV infection cells are refractory to pSTAT1 activation by IFN-II stimulation (Mann et al., 2008; Najarro et al., 2001; Schmidt et al., 2013). Hitherto, this phenotype was mainly attributed to vH1, however deletion of 018 led to an almost complete rescue of pSTAT1 levels despite the presence of vH1, demonstrating that during infection 018, rather than vH1, is responsible for this phenotype. Consistent with this early block, 018 is one of the earliest viral proteins detected during infection (Soday et al., 2019).

Despite apparent redundancy in inhibition of IFN-induced signalling by VACV, deletion of individual IFN antagonists leads to virus attenuation *in vivo* (Figure 4; Symons et al., 1995; Unterholzner et al., 2011). These non-redundant phenotypes may stem from each inhibitor having different locations or expression kinetics or being multifunctional. Unlike intracellular inhibitors, B18 and B8 are secreted from cells and thus can neutralise IFNs extracellularly and distally. Also, B18 can bind to cell surface glycosaminoglycans and thereby inhibit IFN-I-induced signalling in uninfected cells (Alcamí et al., 2000; Montanuy et al., 2011). This is the major mechanism by which B18 contributes to virulence (Hernáez et al., 2018). Although the B18 orthologue from Yaba-like disease virus (a yatapoxvirus) binds and inhibits IFN-III, the VACV B18 protein does not (Huang et al., 2007), and there is no known specific inhibitor of IFN-III-induced signalling made by VACV. Nonetheless, cells infected with VACV are refractory to pSTAT1 induction after IFN-III stimulation, and IFN-III expression during viral infection has little effect on VACV replication (Bandi et al., 2010; Bartlett et al., 2005). These observations may be explained by the action of 018. Differences in expression kinetics of VACV IFN antagonists could also affect redundancy, for, although B18 functions upstream of 018, VACV lacking 018 showed enhanced levels of pSTAT1 after IFN-I stimulation. Lastly, virus proteins are often multifunctional. Indeed VACV protein C6, which inhibits both IFN production (Unterholzner et al., 2011) and IFN-I signalling in the nucleus (Stuart et al., 2016) also degrades HDAC4 and 5, which are restriction factors for VACV, and this might be the major factor contributing to virulence (Lu et al., 2019; Soday et al., 2019).

Deletion of IFN antagonists can improve the safety and immunological memory of VACV-based vaccine vectors (Albarnaz et al., 2018). Modified vaccinia Ankara (MVA) is a widely used VACV-based vaccine vector and expresses 018 (Wennier et al., 2013). MVAs expressing

SARS-CoV-2 proteins have been described as potential vaccine candidates, and thus our findings can inform further development (Chiuppesi et al., 2020; García-Arriaza et al., 2021; Liu et al., 2021).

In summary, we describe a viral mechanism to antagonise IFN-induced signalling by occupancy of the STAT1 SH2 domain to prevent STAT1 receptor association and subsequent ISG expression. The structure of VACV protein 018 complexed with STAT1 illustrates how a viral protein has evolved an unconventional strategy to bind an SH2 domain with high affinity. The biological importance of 018 is shown by its contribution to virus virulence despite the presence of other IFN antagonists. Finally, this study highlights how disparate viruses can evolve highly similar motifs to target a host response that poses a common threat to all viruses.

Acknowledgments

This work was supported by a Wellcome Trust Principal Research Fellowship (090315, to G.L.S.). C.T.C was funded by the BBSRC Doctoral Training Partnership. T.P. was funded by the MRC Doctoral Training Partnership. M.T.A. was funded by a Harry Smith vacation studentship from the Microbiology Society. J.P.S., C.R.C. and H.D.H. were supported by the NIAID Division of Intramural Research.

We thank Diamond Light Source for access to macromolecular crystallography beam line i04 (proposal 25402). We are grateful for access to instrumentation and support by the X-ray crystallographic and Biophysical research facilities at the Department of Biochemistry, University of Cambridge.

513 Henrietta Lacks, and the HeLa cell line that was established from her tumour cells without her
514 knowledge or consent in 1951, have made significant contributions to scientific progress and
515 advances in human health. We are grateful to Henrietta Lacks, now deceased, and to her
516 surviving family members for their contributions to biomedical research.

517 Author contributions

518 Conceptualisation: C.T.C., T.P. and G.L.S.
519 Methodology: C.T.C., T.P. and J.P.S.
520 Formal Analysis: C.T.C., T.P. and J.P.S.
521 Investigation: C.T.C., T.P., J.P.S., C.R.C. and M.T.A.
522 Resources: T.P., M.H., H.D.H. and G.L.S.
523 Data Curation: C.T.C, T.P., J.P.S. and M.H.
524 Writing: Original draft: C.T.C. and T.P.
525 Writing: Reviewing and Editing: C.T.C, T.P., J.P.S., C.R.C., M.T.A., M.H., H.D.H., and G.L.S.
526 Visualisation: C.T.C. and T.P.
527 Supervision: M.H., H.D.H. and G.L.S.
528 Project Administration: C.T.C. and G.L.S.
529 Funding Acquisition: M.H., H.D.H. and G.L.S.

530 Declaration of interests

531 No conflict of interest to declare.

Figures and legends

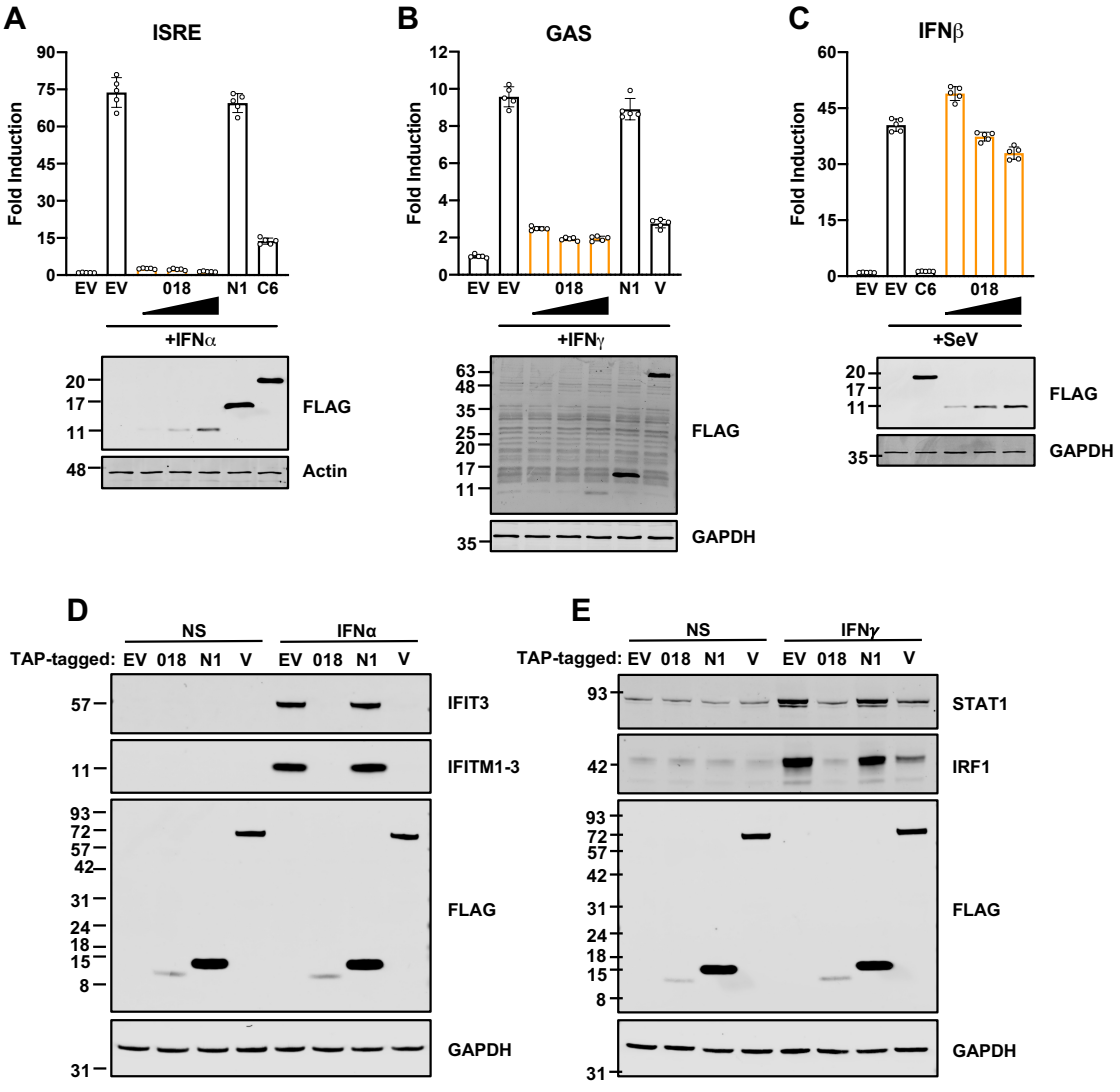

Figure 1. Vaccinia protein 018 inhibits IFN-induced signalling

(A, C) HEK 293T cells or **(B)** HeLa cells were transfected with reporter plasmids ISRE-Luc **(A)**, GAS-Luc **(B),** or IFNβ-Luc **(C)**, plus *TK-Renilla* and vectors expressing proteins indicated fused to a TAP-tag or empty vector (EV). Cells were stimulated with IFNα (1000 U/mL) **(A)**, IFN*γ* (25 ng/mL) **(B)** or SeV **(C)**, for 6 **(A)**, 8 **(B)** or 24 h **(C)** and then luciferase activity was measured. Means ± SD (n=5 per condition) are shown. **(D-E)** T-REx 293 cells were induced with doxycycline (dox, 100 ng/mL) to express indicated proteins. Cells were non-stimulated

(NS) or stimulated with IFNα (1000 U/mL) **(D)** or IFNγ (25 ng/mL) **(E)** for 24 h and lysates were analysed by immunoblotting. Immunoblots were stained against proteins/epitope indicated (**A-E**). Data for (**A-C**) and (**D-E**) are representative of three or two individual experiments, respectively.

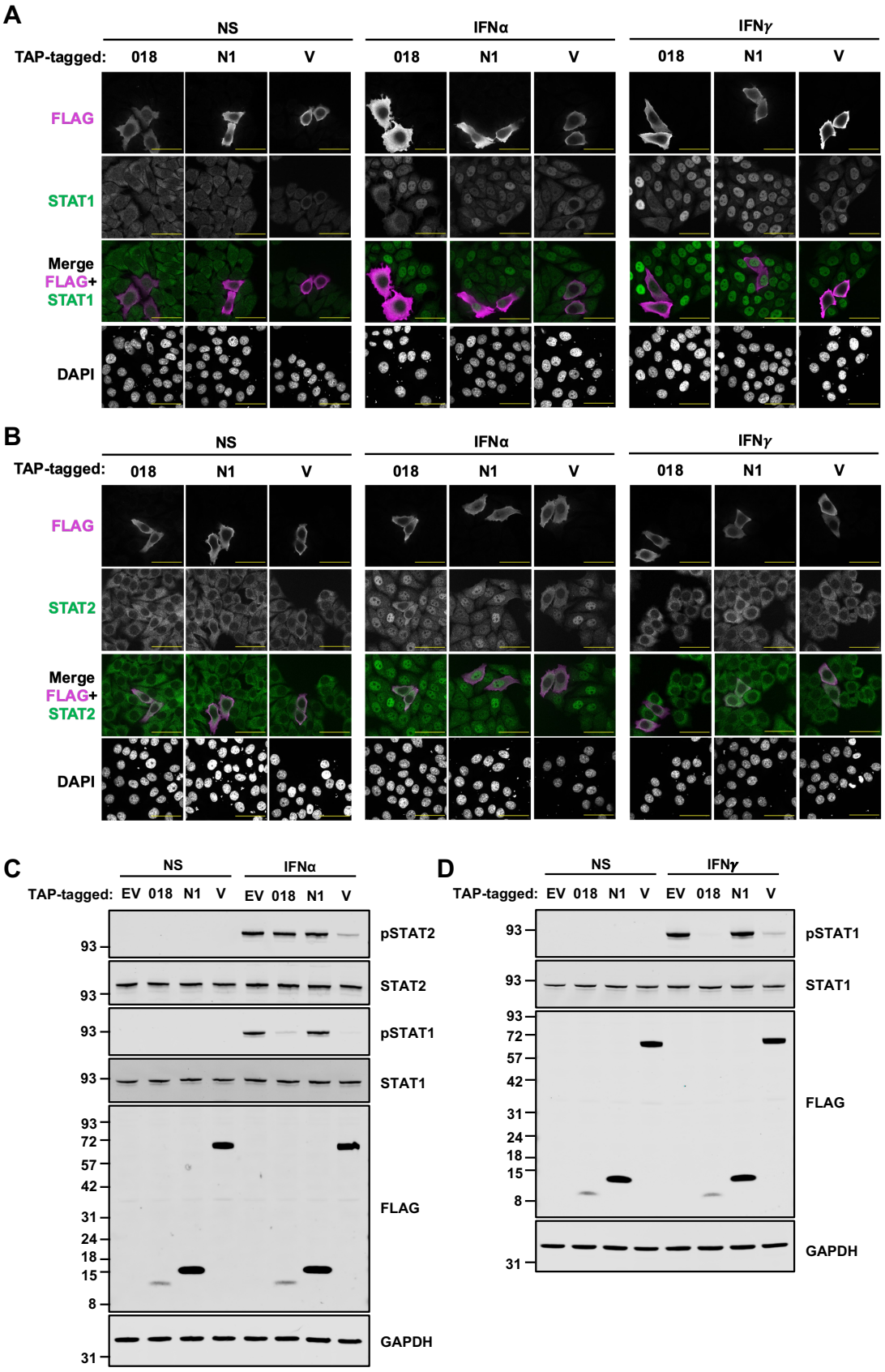

546

Figure 2. Phosphorylation of STAT1 at Tyr 701 is blocked by 018

(**A-B**) HeLa cells were transfected with plasmids expressing TAP-tagged 018, N1 or NiV-V and then were stimulated with IFNα (1000 U/mL) or IFNγ (25 ng/mL) for 1 h. Cells were fixed and permeabilised, and then immunostained with α-FLAG (pink) (**A-B**) and either α-STAT1 (green) (**A**) or α-STAT2 (green) (**B**) and mounted in Mowiol containing DAPI to stain DNA. Cells were visualised by confocal microscopy. Scale bar (yellow) = 50 μm. (**C-D**) T-REx 293 cells were induced with dox (100 ng/mL) to express indicated proteins. Cells were stimulated with IFNα (1000 U/mL) (**C**) or IFNγ (25 ng/mL) (**D**) for 30 min and lysates were analysed by immunoblotting against proteins/epitope indicated. Quantification of band intensities for (**C-D**) is provided in **Figure S2**. Data for (**A-B**) and (**C-D**) are representative of two or three individual experiments, respectively.

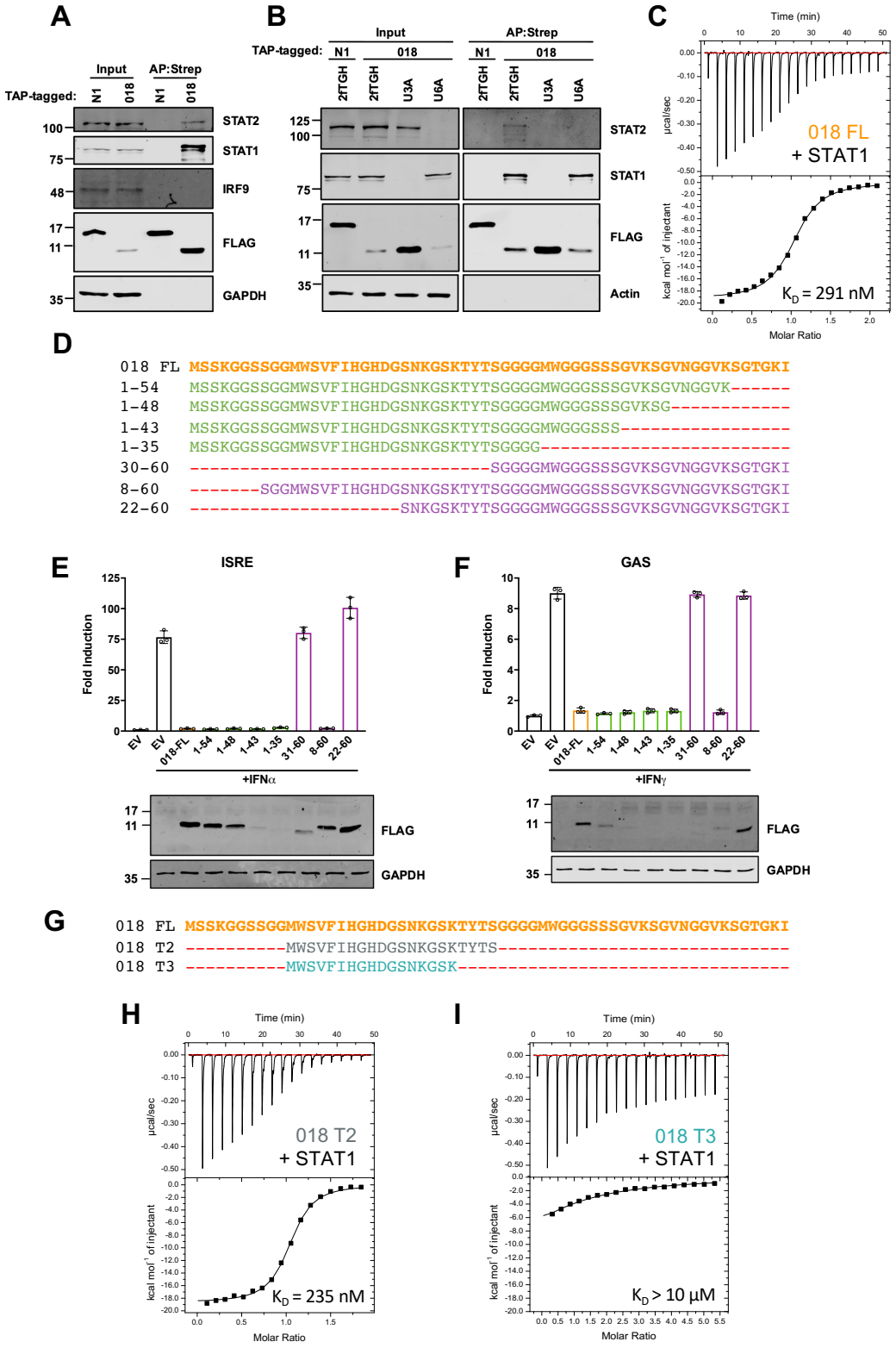

Figure 3. A minimal 21 aa fragment of 018 is sufficient to bind STAT1

(**A-B**) TAP-tagged 018 and N1 were expressed in 2fTGH cells (**A**) or 2fTGH, U3A ($STAT1^{-/-}$) and U6A ($STAT2^{-/-}$) cells (**B**) by transfection and were affinity purified by Strep-Tactin. Whole cell lysate (Input) and affinity purified proteins (AP:Strep) were analysed by immunoblotting. **(C)** ITC data for GB1-018 (100 µM) titrated into U-STAT1 (10 µM). Fitting of the isotherm (bottom) to a one site model gave a K_D of 290 nM. Initial low volume injection is excluded from analysis. Complete fitted ITC parameters are provided in **Table S5**. (**D**) Sequences for TAP-tagged C-terminal (green) and N-terminal (purple) 018 truncation mutants. **(E)** HEK 293T or **(F)** HeLa cells were transfected with reporter plasmids ISRE-Luc **(E)** or GAS-Luc **(F)** along with *TK-Renilla* and vectors from (**D**). Cells were stimulated with IFNα (1000 U/mL) (**E**) or IFNγ (25 ng/mL) (**F**) for 6 (**E**) or 8 h (**F**) and then luciferase activity was measured. Means ± SD (n=3 per condition) are shown. Immunoblots were stained with antibodies against proteins/epitopes indicated (**A-B**) and (**E-F**). Percentage inhibitory activity and relative protein expression levels from figures (**E-F)** are provided in **Figure S3**. Data shown in (**A-B**) and (**E-F**) are representative of three or two individual experiments, respectively. (**G**) Sequences for purified GB1-fused 018 truncation mutants. (**H-I**) ITC data for 150 µM GB1-018^{T2} (**H**) or 350 µM GB1-018^{T3} (**I**) titrated into 150 µM STAT1. Accurate fitting of the isotherm for (**I**) was not possible due to the low C-value of the reaction.

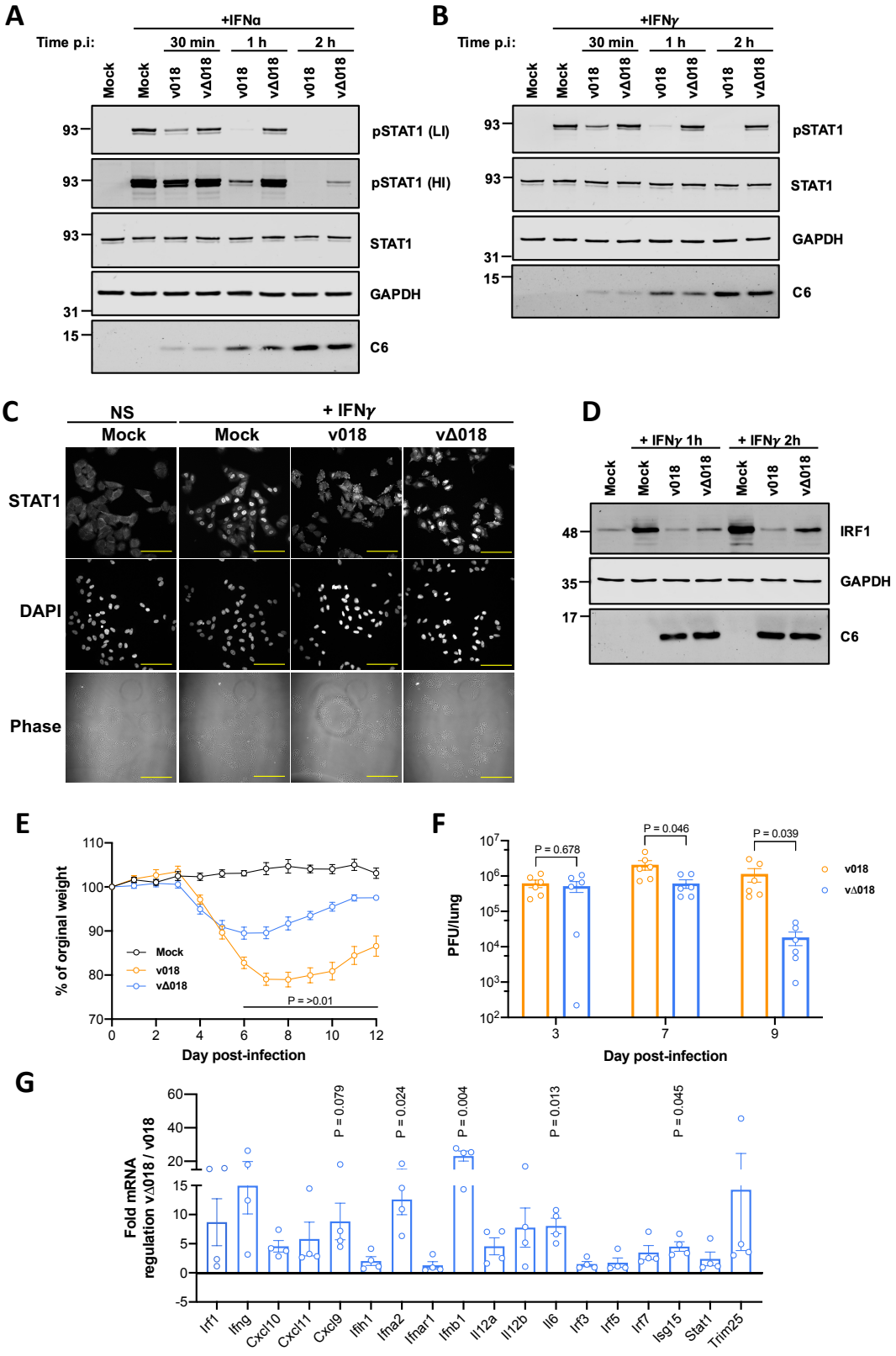

Figure 4. 018 is a virulence factor

582 (**A-B**) A549 cells were mock infected or infected with v018 or vΔ018 at 10 pfu/cell. At 30 min,
583 1 h or 2 h post infection (p.i.) cells were washed once, then stimulated with IFNα (1000 U/mL)
584 (**A**) or IFNγ (25 ng/mL) (**B**) for 30 mins and lysates were analysed by immunoblotting. (**C-D**)
585 A549 cells were infected as described for (**A-B**) and at 2 h p.i., cells were washed once, and
586 then stimulated with IFNγ (25 ng/mL) for 30 mins (**C**), or 1 and 2 h (**D**). (**C**) Cells were fixed
587 and permeabilised then immunostained with α-STAT1 and mounted in Mowiol-containing
588 DAPI to stain DNA and visualised by confocal microscopy. Scale bar (yellow) = 100 µm. (**D**)
589 Cell lysates were analysed by immunoblotting. Immunoblots were stained against proteins
590 indicated including the early VACV protein C6 to control for equal infection (**A-B** and **D**). For
591 (**A**) high intensity (HI) and low intensity (LI) scans for α-pSTAT1 are shown. Data for (**A-D**)
592 are representative of three individual experiments. (**E-G**) Female BALB/c mice 6-10 weeks
593 old were infected via the intranasal route with either v018 (orange) or vΔ018 (blue) at 10^3 (**E-**
594 **F**) or 10^5 (**G**) pfu and weight was measured daily (**E**) or virus titres of upper lungs lobes were
595 measured by plaque assay on days 3, 7 and 9 (**F**), or mice were sacrificed at 3 day p.i. and
596 mRNA levels of indicated genes isolated from upper lung lobes were analysed by RT-qPCR
597 (**G**). Data from (**E-F**) are representative of at two individual experiments using either 5 or 3
598 mice, respectively, per group which were then pooled. Data from (**G**) is representative of 4
599 (vΔ018) or 3 (v018) mice per group. For (**E-G**) means ± SEM are shown, and P values were
600 calculated using Unpaired T-test with (**E-F**) or without (**G**) Welch's correction.
601

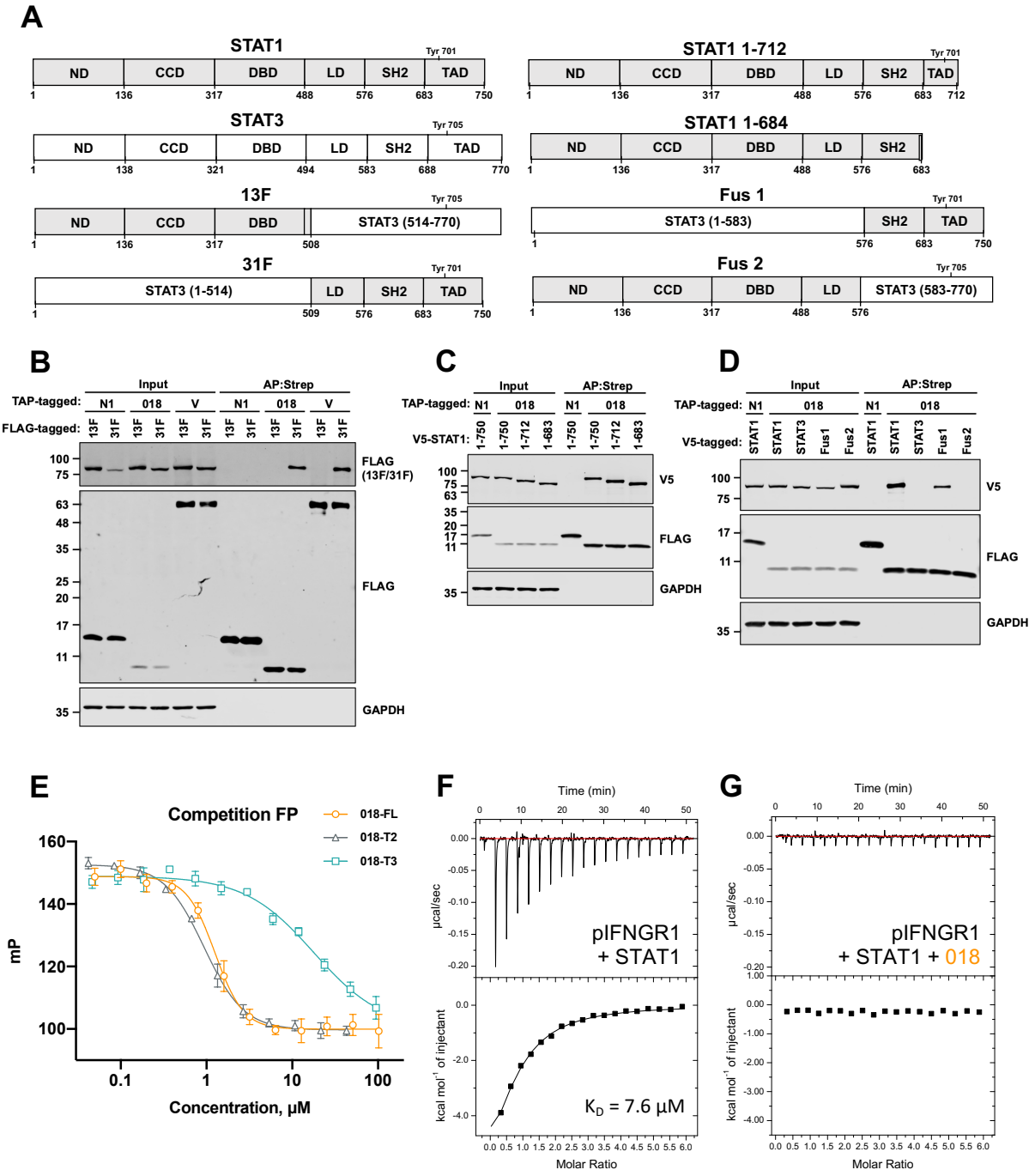

Figure 5. 018 binds the STAT1 SH2 domain to block its association with the phosphorylated IFNGR1

(**A**) Schematic of STAT1-STAT3 chimeras and STAT1 truncation mutants. STAT1 regions (grey) and STAT3 (white) are shown, and domains are annotated as ND (N-terminal domain), CCD (Coiled-coil domain), DBD (DNA-binding domain), LD (Linker-domain), SH2 (Src

608 homology-2-domain), and TAD (Transactivation-domain). (**B-D**) TAP-tagged proteins
609 indicated were co-expressed with either FLAG (**B**) or V5-tagged (**C-D**) STAT proteins from
610 (**A**) by transfection in U3A (STAT1$^{-/-}$) cells and TAP-tagged proteins were purified by Strep-
611 Tactin. Whole cell lysates (Input) and affinity-purified proteins (AP:Strep) were analysed by
612 immunoblotting for the indicated proteins/epitopes. Data from (**B-D**) are representative of two
613 individual experiments. (**E**) Competition FP measurements for GB1-018 and truncation
614 mutants. Each reaction contained 10 nM fluorescein-pIFNGR1 12-mer preincubated with 1.5
615 μM U-STAT1, to which two-fold serial dilutions of purified GB1-018 proteins were added (all
616 concentrations are final values). One hundred mP represents the calibrated FP value of the free
617 fluorescent probe. (**F-G**) ITC data for 300 μM pIFNGR1 5-mer titrated into 100μM U-STAT1
618 (**F**) or 100μM U-STAT1 preincubated with GB1-018 (**G**). No heat of binding was detected for
619 (**G**). Complete fitted ITC parameters are provided in **Table S5**.
620

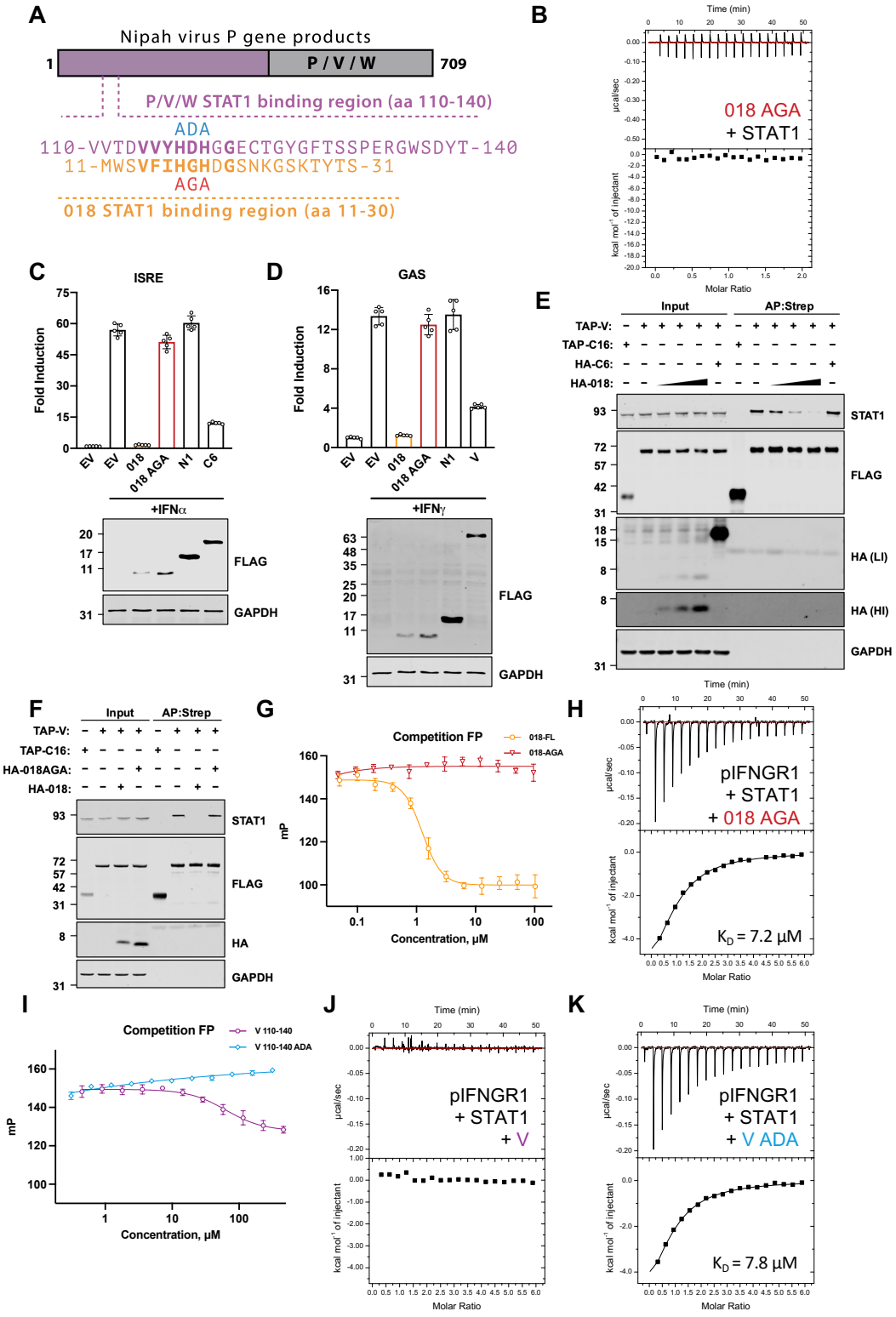

Figure 6. Vaccinia 018 and Nipah virus V protein utilise a shared motif to engage STAT1

(**A**) Schematic of Nipah virus P, V and W proteins encoded by the P gene indicating the common N-terminal region (purple) and unique C-terminal region (dark grey). Below, the STAT1-binding regions of P/V/W (residues 110-140, purple) and 018 (residues. 11-31, orange) are aligned with key conserved residues highlighted in bold. Sites of NiV-V^{ADA} (blue) and 018^{AGA} (red) mutants are shown. (**B**) ITC data for the titration of 100 μM GB1-018^{AGA} into 10 μM U-STAT1. No heat of binding was observed. (**C**) HEK 293T or (**D**) HeLa cells were transfected with reporter plasmids ISRE-Luc **(C)** or GAS-Luc (**D**) along with *TK-Renilla* and vectors expressing the proteins indicated fused to a TAP-tag. Cells were stimulated with IFNα (1000 U/mL) **(C)**, or IFNγ (25 ng/mL) **(D)** for 6 (**C**) or 8 h (**D**) and then luciferase activity was measured. Means ± SD (n=5 per condition) are shown. (**E-F**) TAP-tagged and HA-tagged proteins were co-expressed in HEK 293T cells by transfection as indicted and TAP-tagged proteins were affinity purified by Strep-Tactin. Whole cell lysates (Input) and affinity purified (AP:Strep) proteins were analysed by immunoblotting. For (**E**) high-intensity (HI) and low intensity (LI) scans are shown for α-HA. VACV proteins TAP-C16 and HA-C6 were used as a pulldown and competition protein controls respectively. Immunoblots were stained against proteins/epitopes indicated (**C-F**). Data shown in (**C-D**) and (**E-F**) are representative of two or three individual experiments respectively. (**G**) Competition FP measurements for GB1-018 and GB1-018^{AGA} binding to U-STAT1. Each reaction contained 10 nM fluorescein-pIFNGR1 12-mer preincubated with 1.5 μM U-STAT1, to which two-fold serial dilutions of purified GB1-018 proteins were added (all concentrations are final values). One hundred mP represents the calibrated FP value of the free fluorescent probe. (**H+J+K**) ITC data for 300 μM pIFNGR1 5-mer titrated into 10 μM U-STAT1 preincubated with 50 μM GB1-018^{AGA} (**H**), 200 μM NiV-V (**J**) or 200 μM NiV-V^{ADA} (**K**). No heat of binding was detected for the reaction containing GB1-NiV-V. Complete fitted ITC parameters are provided in **Table S5**. (**I**) Competition FP measurements for GB1-NiV-V and GB1-NiV-V^{ADA} binding to U-STAT1. Each reaction

649 contained 10 nM fluorescein-pIFNGR1 12-mer preincubated with 1.5 μM U-STAT1, to which
650 two-fold serial dilutions of purified GB1-NiV constructs were added (all concentrations are
651 final values). The NiV-V^{ADA} curve has a positive slope at high protein concentrations due to
652 either increased sample viscosity or non-specific interactions. One hundred mP represents the
653 calibrated FP value of free fluorescent probe.
654

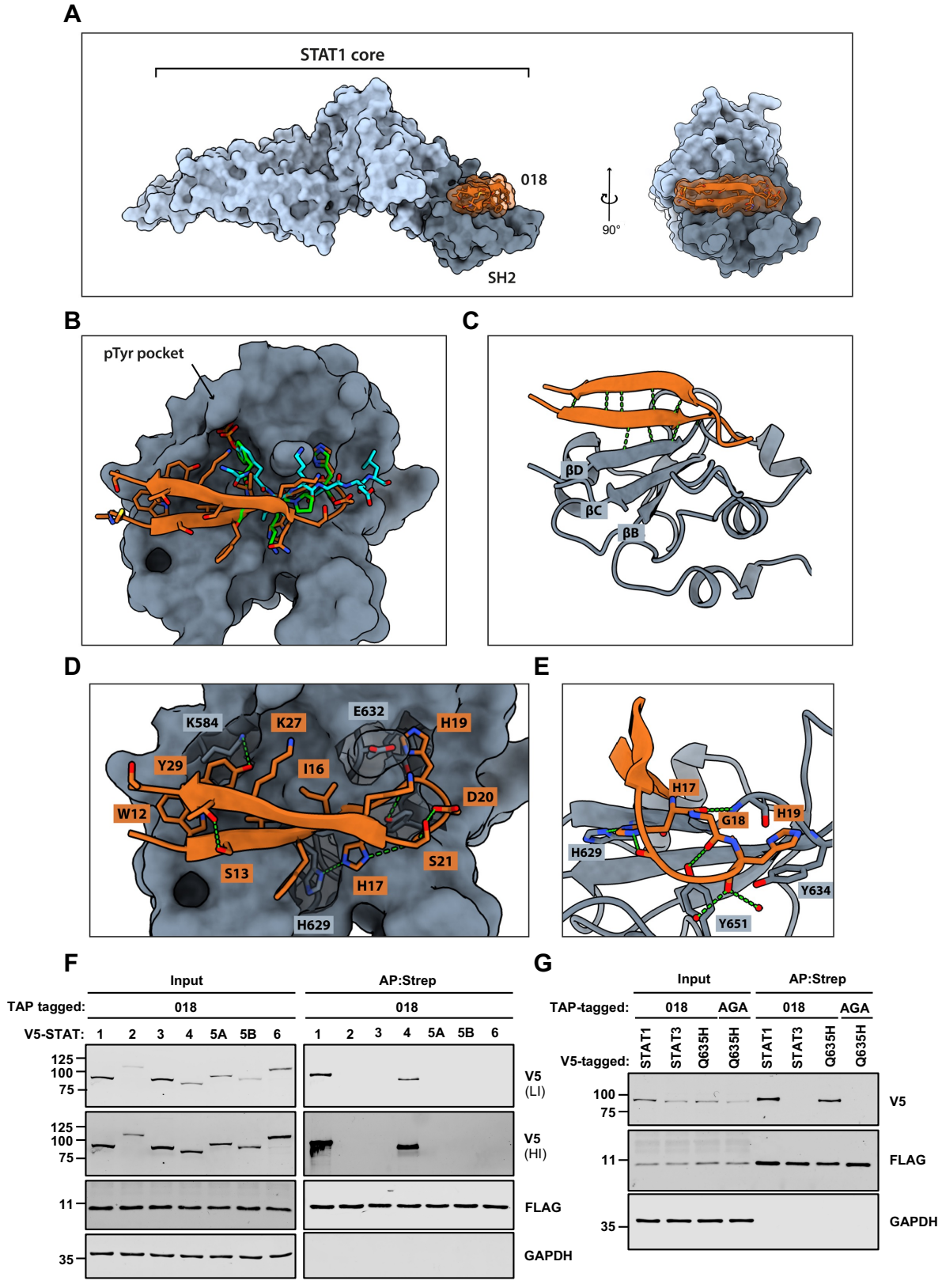

Figure 7. Structural basis of 018 binding to U-STAT1

A crystal structure was determined for 018:STAT1 core fragment complex (PDB: 7nuf). In all images, 018 is depicted in orange, the SH2 domain is dark grey and the rest of the core fragment is light grey. (**A**) Surface representation of the complex viewed from two perpendicular axes. (**B**) 018 binding mode at the STAT1 SH2 domain superimposed with IFNGR1 phosphopeptide (green, PDB: 1yvl) and STAT1 pTyr701 phosphopeptide (cyan, PDB: 1bf5). (**C**) Ribbon representation of 018 and the STAT1 SH2 domain with β-sheet-forming hydrogen bonds depicted in green. SH2 domain core β-strands are labelled according to conventional nomenclature. (**D**) Detailed depiction of 018 binding to the STAT1 SH2 domain. 018 sidechains are depicted as sticks, while backbone atoms are represented by a ribbon cartoon. Key STAT1 sidechains are depicted as sticks under semi-transparent surface. (**E**) A zoomed view of HxH motif binding. (**F, G**) V5-tagged and TAP-tagged proteins were co-expressed in U3A ($STAT1^{-/-}$) cells by transfection as indicted in the figure and TAP-tagged proteins were affinity purified using Strep-Tactin. Whole cell lysates (Input) and affinity purified proteins (AP:Strep) were analysed by immunoblotting against the indicated proteins/epitope. $STAT3^{Q635H}$ and 018^{AGA} are labelled as Q635H and AGA, respectively (**G**). For (**F**) high (HI) and low intensity (LI) scans of α-V5 are shown. Data shown in (**F, G**) are representative of two individual experiments.

676 # STAR methods

677 ## KEY RESOURCES TABLE

678

REAGENT or RESOURCE	SOURCE	IDENTIFIER
Antibodies		
Rabbit anti-STAT1	Cell Signaling Technologies	14994 RRID:AB_2737027
Rabbit anti-STAT2	Cell Signaling Technologies	72604 RRID:AB_2799824
Rabbit anti-IRF9	Cell Signaling Technologies	76684 RRID:AB 2799885
Rabbit anti-pSTAT1 (Tyr 701)	Cell Signaling Technologies	9167 RRID:AB_561284
Rabbit anti-pSTAT2 (Tyr 690)	Cell Signaling Technologies	88410 RRID:AB_2800123
Rabbit anti-IRF1	Cell Signaling Technologies	8478 RRID:AB_10949108
Mouse anti-IFIT3	Santa Cruz	sc-393512 RRID:AB_2857847
Mouse anti-IFITM1-3	Santa Cruz	sc-374026 RRID:AB_10916884
Rabbit anti-C6	Laboratory of Geoffrey L Smith; Unterholzner et al., 2011	N/A
Mouse anti-GAPDH	Sigma-Aldrich	G8795 RRID:AB_1078991
Rabbit anti-actin	Sigma-Aldrich	A2066 RRID:AB_476693
Mouse anti-FLAG	Sigma-Aldrich	F3165; RRID:AB_259529
Mouse anti-HA	Biolegend	901513; RRID:AB_2565335
Rabbit anti-V5	Cell Signaling Technologies	13202; RRID:AB_2687461
IRDye 680RD-conjugated goat anti-rabbit IgG	LI-COR	926-68071; RRID:AB_10956166
IRDye 680LT-conjugated goat anti-mouse IgG	LI-COR	926-68020; RRID:AB_10706161
IRDye 800CW-conjugated goat anti-rabbit IgG	LI-COR	926-32211; RRID:AB_621843
IRDye 800CW-conjugated goat anti-mouse IgG	LI-COR	926-32210; RRID:AB_621842
Donkey anti-Mouse IgG (H+L) secondary antibody, Alexa Fluor 546	Molecular Probes	A10036; RRID:AB_2534012
Goat anti-Rabbit IgG (H+L) secondary antibody, Alexa Fluor 488	Molecular Probes	A11008; RRID:AB_143165
Bacterial and virus strains		
T7 Express competent *E. coli*	New England Biolabs	C2566I
E. coli (subcloning efficiency DH5α competent Cells)	Invitrogen	18265-017
VACV strain Western Reserve: v018	This paper	N/A
VACV strain Western Reserve: vΔ018	This paper	N/A
VACV strain Western Reserve: vTAP-018	This paper	N/A
VACV strain Western Reserve: vTAP-N1	Laboratory of Geoffrey L Smith (Maluquer de Motes et al., 2014)	N/A
Sendai virus (SeV) strain Cantell	A gift from Steve Goodbourn (St George's Hospital Medical School, University of London) Licence No. ITIMP17.0612A	N/A

Chemicals, peptides, and recombinant proteins		
Fluor-pIFNGR1 12-mer peptide (5Flu-GTSFGpYDKPHVLV-NH2)	PeptideSynthetics (UK)	https://www.peptidesynthetics.co.uk/
pIFNGR1 5-mer peptide (Ac-pYDKPH-NH2)	Genosphere Biotechnologies	https://www.genosphere-biotech.com/
018 21-mer peptide (Ac-MWSVFIHGHDGSNKGSKTYTS-NH2)	Genosphere Biotechnologies	https://www.genosphere-biotech.com/
Full-length STAT1 protein	This paper	N/A
GB1-018 protein fusions	This paper	N/A
GB1-NiV-V protein fusions	This paper	N/A
$STAT1^{136-684,\Delta183-190,H182A,E393A,E394A}$ protein	This paper	N/A
DMEM	Gibco	41966-029
MEM	Gibco	31095-029
MEM NEAAs	Gibco	11140050
Trypsin-EDTA	Gibco	25300-054
Penicillin-streptomycin	Gibco	15140-122
Fetal bovine serum (FBS)	PAN-Biotech	P30-19375
Opti-MEM I reduced serum medium	Gibco	51985-026
Bovine serum albumin (BSA)	Sigma-Aldrich	A3059
Blasticidin S HCl solution	Santa Cruz	sc-495389
Zeocin	InvivoGen	ant-zn-1
Xanthine sodium salt	Sigma-Aldirch	x3627
Hypoxanthine	Sigma-Aldrich	H9377
Mycophenolic acid	Sigma-Aldrich	M5255
Agarose (low gelling temperature)	Sigma-Aldrich	A4018
Doxycycline hydrochloride	Melford	D43020
cOmplete, EDTA-free protease inhibitor cocktail	Roche	11836153001
PhosSTOP phosphatase inhibitor cocktail	Roche	04906837001
16% Paraformaldehyde aqueous solution, EM grade	Electron Microscopy Sciences	15710
IFNa 2 human	Sigma-Aldrich	SRP4594
IFNγ human	PreproTech	300-02
DNase I	Sigma-Aldrich	DN25
DAPI (4',6-diamidino-2-phenylindole)	Biotium	40043
Mowiol 4-88	Calbiochem	475904
Polyethylenimine (PEI), linear, MW 25000	Polysciences	23966
Passive lysis 5X buffer	Promega	E1941
Acetyl coenzyme A (firefly luciferase reagents)	Nanolight Technology	315-500
Luciferin (firefly luciferase reagent)	Nanolight Technology	306-500
Coelenterazine (*Renilla* luciferase reagent)	Nanolight Technology	303-10
Hanks' balanced salt solution (HBSS)	Lonza	10-527F
Collagenase (type I)	Worthington Biochemicals	LS004216
Crystal violet	Sigma-Aldrich	C0775
Formaldehyde	Sigma-Aldrich	252549

Gentamicin (50 mg/mL)	Sigma-Aldrich	G1397
Carboxymethylcellulose sodium salt	Sigma-Aldrich	419273
TCEP	Melford	T26500
TEV protease	Prepared in-house from the pRK793 expression plasmid (Addgene #8827)	N/A
AEBSF	Melford	A20010
PEG 3350	Sigma-Aldrich	202444
Ni-NTA agarose	Cube Biotech	31103
Critical commercial assays		
Pierce BCA protein assay kit	Thermo Fisher Scientific	23227
MycoAlert mycoplasma detection kit	Lonza	LT07-218
Q5 High-fidelity DNA polymerase	New England Biolabs	M0491
Q5 Site-directed mutagenesis kit	New England Biolabs	E0554
One*Taq* Quick-load 2X master mix with standard buffer	New England Biolabs	M486
T4 DNA ligase	New England Biolabs	M0202
*Trans*IT-LT1	Mirus Bio	MIR 2305
Monarch Total RNA miniprep kit	New England Biolabs	T2010
Luna Universal one-step RT-qPCR kit	New England Biolabs	E3005
Strep-TactinXT superflow resin	IBA	2-4030-002
Anti-FLAG M2 affinity gel	Sigma-Alrich	A220
TnT coupled wheat germ extract (SP6)	Promega	L4130
Lysing matric S (1/8") metal beads	MPBio	116925100
Qiagen RNeasy mini kit	Qiagen	74104
RT^2 First stand kit	Qiagen	330404
Antiviral response qPCR array	Qiagen	PAMM-122Z-24
RT^2 SYBR Green ROX qPCR mastermix	Qiagen	330523
RT^2 qPCR primer assay for mouse IRF1	Qiagen	PPM03203D-200
RT^2 qPCR primer assay for mouse IFNγ	Qiagen	PPM03121A-200
RT^2 qPCR primer assay for mouse Actb	Qiagen	PPM02945B-200
RT^2 qPCR primer assay for mouse B2M	Qiagen	PPM03562A-200
RT^2 qPCR primer assay for mouse GAPDH	Qiagen	PPM02946E-200
Deposited data		
Structure of 018 complexed with STAT1 core fragment	This paper	PDB ID: 7nuf
Experimental models: Cell lines		
BS-C-1	ATCC	CCL-26
CV-1	ATCC	CCL-70
RK13	ATCC	CCL-37
MEF	A gift from Prof. Dr Eugen Kerkhoff – University Hospital Regenburg, Germany	N/A
HEK 293T	ATCC	CRL-11268
HeLa	ATCC	CCL-2

T-REx 293	Life Technologies	R71007
T-REx 293 EV	This paper	N/A
T-REx 293TAP-N1	This paper	N/A
T-REx 293TAP-018	This paper	N/A
T-REx 293 TAP-NiV-V	This paper	N/A
A549	ATCC	CCL-185
2fTGH	Sigma Aldrich	12021508
U3A	Sigma-Aldrich	12021503
U6A	Sigma Aldrich	12021507
TK$^-$ 143B	ATCC	CRL-8303
Experimental models: Organisms/strains		
BALB/c mice, female, adult aged 6-10 weeks old	Taconic Farms	Mouse strain: BALB/CANNTAC
Oligonucleotides		
Primers for construction of recombinant DNA	See Table S1	N/A
Primers for RT-qPCR (cell culture)	See Table S2	N/A
Primers for analytical PCR or sequencing	See Table S3	N/A
Recombinant DNA		
pcDNA4/TO	Thermo Fisher Scientific	V102020
pcDNA4/TO TAP-018	This Paper	N/A
pcDNA/TO TAP-NiV-V	This Paper	N/A
pcDNA/TO TAP-N1	Laboratory of Geoffrey L Smith (Maluquer de Motes et al., 2011)	N/A
pcDNA4/TO TAP-C6	Laboratory of Geoffrey L Smith (Stuart et al., 2016)	N/A
pcDNA4/TO TAP-C16	Laboratory of Geoffrey L Smtih (Peters et al., 2013)	N/A
pcDNA4/TO TAP-018 (1-54)	This Paper	N/A
pcDNA4/TO TAP-018 (1-48)	This Paper	N/A
pcDNA4/TO TAP-018 (1-43)	This Paper	N/A
pcDNA4/TO TAP-018 (1-35)	This Paper	N/A
pcDNA4/TO TAP-018 (1-30)	This Paper	N/A
pcDNA4/TO TAP-018 (1-27)	This Paper	N/A
pcDNA4/TO TAP-018(1-24)	This Paper	N/A
pcDNA4/TO TAP-018 (1-21)	This Paper	N/A
pcDNA4/TO TAP-018 (8-60)	This Paper	N/A
pcDNA4/TO TAP-018 (11-60)	This Paper	N/A
pcDNA4/TO TAP-018 (14-60)	This Paper	N/A
pcDNA4/TO TAP-018 (17-60)	This Paper	N/A
pcDNA4/TO TAP-018 (22-60)	This Paper	N/A
pcDNA4/TO TAP-018 (31-60)	This Paper	N/A
pcDNA4/TO TAP-018^{AGA}	This Paper	N/A
pcDNA3 HA-C6	Laboratory of Geoffrey L Smith (Unterholzner et al., 2011)	N/A

pcDNA3 HA-018	This Paper	N/A
pcDNA3 HA-018^{AGA}	This Paper	N/A
pcDNA3 V5-STAT1	This Paper	N/A
pcDNA3 V5-STAT2	This Paper	N/A
pcDNA3 V5-STAT3 (human)	This Paper	N/A
pcDNA3 V5-STAT3 (mouse)	This Paper	N/A
pcDNA3 V5-STAT4	This Paper	N/A
pcDNA3 V5-STAT5A	This Paper	N/A
pcDNA3 V5-STAT5B	This Paper	N/A
pcDNA3 V5-STAT6	This Paper	N/A
pcDNA3 V5-STAT1 (1-712)	This Paper	N/A
pcDNA3 V5-STAT1 (1-684)	This Paper	N/A
pcDNA3 V5-Fus1	This Paper	N/A
pcDNA3 V5-Fus2	This Paper	N/A
pcDNA3 V5-STAT3^{Q635H} (human)	This Paper	N/A
13F	A gift from Curt Horvath (Northwestern University, USA)	N/A
31F	A gift from Curt Horvath (Northwestern University, USA)	N/A
ISRE-Luc	Promega	E4141
GAS-Luc	A gift from Andrew Bowie (Trinity College Dublin, Republic of Ireland)	N/A
IFNβ-Luc	A gift from T. Taniguchi (University of Tokyo, Japan)	N/A
TK-Renilla-Luc	Promega (GL3-*Renilla* vector was made by replacing the firefly luciferase ORF from pGL3-control (Promega) with the *Renilla* luciferase ORF from pRL-TK (Promega)	E2241
pF3A	Promega	L5671
pF3A TAP-018	This Paper	N/A
pF3A STAT1	This Paper	N/A
pF3A TAP-K7	Laboratory of Geoffrey L Smith (Torres et al., 2020)	N/A
pUC13-Ecogpt-EGFP Δ018	This Paper	N/A
pUC13-Ecogpt-EGFP TAP-018	This Paper	N/A
pOPTH	(Teo et al., 2004)	N/A
pOPTH-TEV	This Paper	N/A
pOPTH-TEV-STAT1$^{136-684,Δ183-190,H182A,E393A,E394A}$	This Paper	N/A
pEXP-nHis	Laboratory of Marko Hyvonen	Addgene #112558
pEXP-nHis-STAT1	This Paper	N/A
pPEPT	Laboratory of Marko Hyvonen	N/A
pPEPT 018	This Paper	N/A
pPEPT 018^{T2}	This Paper	N/A
pPEPT 018^{T3}	This Paper	N/A
pPEPT 018^{AGA}	This Paper	N/A
pPEPT NiV-V (110-140)	This Paper	N/A
pPEPT NiV-V (110-140)^{ADA}	This Paper	N/A

Software and algorithms		
Image Studio Lite Quantification Software	LI-COR Biosciences	https://www.licor.com/bio/image-studio-lite/
MARS Data Analysis Software	BMG LABTECH	https://www.bmglabtech.com/mars-data-analysis-software/
ImageJ-Fiji	(Schindelin et al., 2012)	https://imagej.net/software/fiji/
QuantStudio Software	Applied Biosystems	https://www.thermofisher.com/uk/en/home/technical-resources/software-downloads/applied-biosystems-viia-7-real-time-pcr-system.html
Origin for ITC200	Malvern Instruments	https://www.malvernpanalytical.com/en
autoProc	(Vonrhein et al., 2011)	https://www.globalphasing.com/autoproc/
Phenix.refine	(Liebschner et al., 2019)	https://www.phenix-online.org/
autoBuster	(Smart et al., 2012)	https://www.globalphasing.com/buster/
Prism	GraphPad	https://www.graphpad.com/scientific-software/prism/
GeneGlobe Data Analysis Centre	Qiagen	https://geneglobe.qiagen.com/us/analyze
Coot	(Emsley et al., 2010)	https://www2.mrc-lmb.cam.ac.uk/personal/pemsley/coot/
ChimeraX	UCSF	https://www.rbvi.ucsf.edu/chimerax/
ASTRA	Wyatt Technology	https://www.wyatt.com/
Uniprot	(Bateman, 2019)	https://www.uniprot.org/
NCBI blast	(Johnson et al., 2008)	https://blast.ncbi.nlm.nih.gov/Blast.cgi
Clustal Omega	(McWilliam et al., 2013)	https://www.ebi.ac.uk/Tools/msa/clustalo/
ESPrit 3.0	(Robert and Gouet, 2014)	https://espript.ibcp.fr

RESOURCE AVAILABILITY

Lead contact

Further information and requests for resources and reagents should be directed to and will be fulfilled by the lead contact, Geoffrey L Smith (gls37@cam.ac.uk).

Materials availability

See above.

Data and code availability

018:STAT1 X-ray crystallographic structure has been deposited on the PDB under the accession code 7nuf.

EXPERIMENTAL MODEL AND SUBJECT DETAILS

Cell lines

BS-C-1 (ATCC), CV-1 (ATCC), MEFs (A gift from Prof. Dr Eugen Kerkhoff), HEK 293T (ATCC), A549 (ATCC), 2fTGH (a human cell line containing the selectable marker guanine phosphoribosyltransferase regulated by IFN-α, Sigma-Aldrich), U3A (a 2fTGH derived STAT1$^{-/-}$ cell line, Sigma-Aldrich), U6A (a 2fTGH derived, STAT2$^{-/-}$ cell line, Sigma-Aldrich), and TK^{-} 143B cells (ATCC) were maintained in DMEM (Gibco) supplemented with 10% fetal bovine serum (FBS, PAN-Biotech) and penicillin-streptomycin (PS, 50 µg/mL, Gibco). T-REx 293 cells (Life technologies) were maintained in DMEM supplemented with 10% FBS, PS (50 µg/mL) and blasticidin (10 µg/mL, Santa Cruz), and T-REx 293 derived cells lines expressing EV, TAP-N1, TAP-018, or TAP-NiV-V were further supplemented with zeocin (100 ug/mL, Invivogen). HeLa (ATCC) and RK13 cells (ATCC) were maintained in MEM (Gibco) supplemented with 10% FBS, PS (50 µg/mL) and 1% non-essential amino acids (Gibco). The construction of T-REx 293 cell lines expressing proteins inducibly is outlined in the methods detail section.

Viruses

Recombinant vTAP-N1 was derived from VACV strain WR (VACV-WR, GenBank: AY243312.1) (Maluquer de Motes et al., 2014). v018, vΔ018 and vTAP-018 described in this paper were all derived from VACV strain WR and their construction is outlined in the methods detail section.

Animals

Specific pathogen-free BALB/c mice were obtained from Taconic Farms. 6-10 weeks old female mice were used in all experiments. Mice were housed under specific pathogen-free conditions (including negativity for murine norovirus, mouse parvovirus, and mouse hepatitis virus) and were maintained on standard rodent chow and water supplied *ad libitum*. All animal studies were approved by and performed in accordance with the Animal Care and Use Committee of the National Institute of Allergy and Infectious Diseases, USA.

QUANTIFICATION AND STATISTICAL ANALYSIS

Significances were calculated in Prism (GraphPad) by either Dunnett's T3 multiple comparisons test or Unpaired t-test with Welch's correction as indicated. For anti-viral array data (**Figure 4G**), analysis and Unpaired t-tests was performed using GeneGlobe Data Analysis Centre (Qiagen). All significances are indicated with P values.

METHOD DETAILS

Orthologue alignments

Identifiers for poxvirus genomes from which the amino acids sequences of 018 orthologues were derived: vaccinia strain Western Reserve (VACV-WR, GenBank: AY243312.1), Modified vaccinia Ankara (MVA, GenBank: AY603355.1), variola virus (VARV, GenBank:

X69198.1), monkeypox virus (MPXV, GenBank: AF380138.1), cowpox virus strain Brighton Red (CPXV-BR, GenBank: AF482758.2), ectromelia virus (ECTV, GenBank: AF012825.2), camelpox virus (CMLV, GenBank: AF438165.1), rabbitpox virus (RPXV, GenBank: AY484669.1), raccoonpox virus (RCNV, GenBank: KP143769.1), skunkpox virus (SKPTV, GenBank: KU749310.1), taterapox virus (TATV, GenBank: DQ437594.1), Cotia virus (COTV, GenBank: HQ647181.2), Yoka poxvirus (YKPV, GenBank: HQ849551.1). Alignments were performed using Clustal Omega (McWilliam et al., 2013) and conservation annotation was performed using ESPirt 3.0 (Robert and Gouet, 2014).

Plasmids

The 018 open reading frame was codon-optimised for expression in human cells and was synthesised by Gene Art (Thermo Fisher Scientific). All plasmids are described in recombinant DNA key resource table and primers used for construction in **Table S1**.

Construction of T-REx 293 cell lines expressing proteins inducibly

T-REx 293 were transfected with pcDNA4/TO expression plasmids (pcDNA4/TO (EV), pcDNA4/TO TAP-018, pcDNA4/TO TAP-N1 and pcDNA4/TO TAP-NiV-V) using Transit-LT1 (Mirus Bio). Prior to transfection, pcDNA4/TO expression plasmids were linearised using *PvuI* (NEB) to decrease the potential for plasmid-chromosomal integration within the viral ORF. Cells with integrated plasmid were selected in the presence of blasticidin (10 μg/mL) and zeocin (100 μg/mL) and single clones were obtained by limiting dilution. Clones were amplified and lysates were analysed for the expression of TAP-tagged protein by immunoblotting.

754 The expression of TAP-tagged proteins from T-REx 293-derived cells was induced by addition
755 of doxycycline (100 ng/mL, Santa Cruz) to the medium for 24 h for all experiments.
756
757 Construction of recombinant VACVs
758 Recombinant VACVs (vΔ018 and vTAP-018) were constructed using transient dominant
759 selection (Falkner and Moss, 1990). To construct the pUC13_Ecogpt_EGFP_Δ018 plasmid to
760 remove the entire 018 ORF, the downstream (301 bp) and upstream (300 bp) flanking regions
761 of the 018 ORF were amplified by PCR from purified VACV (strain WR) DNA. A 15 bp
762 complementary sequence was added to the internal upstream and downstream primers to
763 facilitate joining of the two-flanking regions by overlapping PCR. The resulting PCR product
764 was then ligated into pUC13- Ecogpt-EGFP using *Pst*I (NEB) and *Bam*HI (NEB) cloning sites.
765 To construct the pUC13-Ecogpt-EGFP TAP-018 plasmid, the downstream flanking and 018
766 ORF (484 bp) and the upstream region of the ORF (300 bp) were amplified by PCR separately
767 from purified VACV (strain WR) DNA. The 018 ORF plus downstream flanking region PCR
768 product was ligated into pcDNA4/TO vector containing an N-terminal TAP-tag using *Not*I
769 (NEB) and *Xba*I (NEB) as an intermediate cloning step. The N-terminal TAP tag fused 018
770 ORF + downstream flanking region was then amplified by PCR using primers that added a 20-
771 bp overhang sequence complementary to the upstream flanking PCR product. The two PCR
772 products were then joined by overlapping PCR and the product was ligated into
773 pUC13_Ecogpt_EGFP using *Pst*I and *Bam*HI cloning sites.
774
775 To construct vΔ018, CV-1 cells were seeded in a T-25 flask to be 70 % confluent the following
776 day. CV-1 cells were then infected with VACV (strain WR) at 0.05 pfu/cell and after 1 h 30
777 min, the inoculum was removed and cells were transfected with 7.5 μg of

778 pUC13_Ecogpt_EGFP_Δ018 using Transit-LT1 (Mirus Bio). Two days p.i., the majority of
779 cells displayed cytopathic effect and were harvested by scrapping cells into the culture medium.
780 Cells were sedimented by centrifugation (500 RCF) and resuspended in 0.5 mL of infection
781 medium (DMEM supplemented with 2% FBS and PS (50 µg/mL). Samples were freeze-
782 thawed three times to lyse cells and release progeny virus and sonicated to disperse particulate
783 material. A series of progeny virus dilutions (10^{-1}, 10^{-2} and 10^{-3} diluted in infection medium)
784 were used to inoculate BS-C-1 cells in 6-well plates that had been preincubated in infection
785 medium, supplemented with mycophenolic acid (25 µg/mL; MPA, Sigma-Alrich), xanthine
786 (250 µg/mL; X, Sigma-Alrich) and hypoxanthine (15 ug/mL; HX, Sigma-Alrich) for 24 h.
787 After 1 h 30 min, the inoculum was removed and replaced with a MEM, 1% (w/v) low gelling
788 temperature agarose (Sigma Alrich), supplemented with MPA, HX, and X. After three days,
789 EGFP-expressing plaques were picked, representing virus that had integrated the pUC13-
790 Ecogpt-EGFP-Δ018, and then further plaque purified in the absence of MPA, HX and X. The
791 genotype of these plaques was then determined by PCR using primers that flank the 018 ORF
792 (**Table S3**) and VACVs containing the desired mutation (vΔ018) or wild type genotype were
793 isolated. vTAP-018 was produced using the same strategy as described above, except that
794 vΔ018 was used as the parental VACV into which the TAP-018 ORF was inserted at its natural
795 locus. Stocks of VACVs were grown in RK13 cells and titrated by plaque assay on BS-C-1
796 cells.
797
798 Purification of VACVs by sedimentation through sucrose
799 VACVs were purified by two rounds of ultracentrifugation through a sucrose cushion as
800 described (Joklik, 1962) and stocks were resuspended in 1 mM Tris-HCl pH 9.0 for cell culture

work or in Hank's balanced salt solution (HBSS) + 0.1% BSA for *in vivo* work. Virus titres were determined by plaque assay.

Viral DNA for vΔ018 and wild-type sibling virus v018 was isolated from sucrose purified virus stocks by phenol:chloroform extraction. Whole genome sequencing of viruses was performed by MircobesNG and virus sequences were aligned to VACV strain WR reference genome (VACV-WR, GenBank: AY243312.1).

VACV infection for cell culture

Virus inoculums were prepared in DMEM supplemented with 2% FBS (infection medium) and virus adsorption was performed at 4 °C for 1 h with gentle agitation every 10 mins. At time 0 h p.i., virus inoculum was removed and replenished with infection medium, and infection was continued at 37 °C.

Virus growth and spread assays

For virus growth curves, BS-C-1 cells were grown to confluence in T-25 flask then infected at 5 pfu/cell. At 1, 8 and 24 h p.i., extracellular and cell-associated virus were harvested by collecting either the supernatant or cell monolayers, respectively. Supernatants were cleared by centrifugation (21,000 RCF) to remove detached cells and debris. Cell monolayers were scrapped into new medium and subjected to three cycles of freeze-thawing followed by sonication to release intracellular virus. Viral titres were determined by plaque assay.

Virus spread was determined by analysis of plaque size growth. Confluent BS-C-1 and RK13 cells in 6-well plates were infected with 30 pfu/per well. At 1 h p.i., medium was replaced with

a semi-solid MEM overlay supplemented with, L-glutamine, 2% FBS and 1.5 % (w/v) carboxymethylcellulose (Sigma-Aldrich). At 72 h p.i., the semi-solid overlay was removed, and monolayers were stained with crystal violet (Sigma-Aldrich).

Immunoblotting

For immunoblotting analysis, cells were washed once in chilled PBS and harvested on ice by scrapping into lysis buffer (Tris pH 8.0, 150 mM NaCl and 1% NP-40, supplemented with protease (cOmplete Mini, Roche) and phosphatase inhibitors (PhosSTOP, Roche). Cell lysates were incubated with rotation at 4 °C for 15 mins before being cleared by centrifugation (21,000 RCF) and protein concentrations were determined using BCA Protein Assay (Pierce). Lysates were mixed with 4X SDS-gel loading buffer and incubated at 100 °C for 5 min to denature protein. Samples were briefly centrifuged (17,000 RCF) before loading onto either SDS-polyacrylamide gels or NuPAGE (4 to 12%, 1 mm, Bis-Tris gels (Thermo Fisher Scientific) along with protein ladder (Abcam) and separated by electrophoresis. Protein gels were incubated in transfers buffer (25 mM Tris, 250 mM glycine, 20% (v/v) methanol) with agitation for 15 min. Gels were transferred onto a nitrocellulose transfer membrane (0.2 μM pore size, GE Healthcare) using a semi-dry transfer system (Trans-tubro blot, BioRad). Nitrocellulose membranes were allowed to dry for 30 mins and then blocked with 5% (w/v) BSA (Sigma), in TBS containing 0.1% Tween-20 for 1 h at room temperature (RT). Primary antibodies (see Key Resources Table) were diluted in blocking buffer and incubated with membranes overnight at 4 °C. Membranes were probed with fluorophore-conjugated secondary antibodies (LI-COR Biosciences) diluted in 5% (w/v) non-fat milk in PBS containing 0.1 % (v/v) Tween-20 and incubated at RT for 45 min. Membranes were imaged using the Odyssey CLx imagining system

(LI-COR Biosciences). Protein band intensities were quantified using Image Studio software (LI-COR Biosciences).

Reporter gene assays

HeLa cells (for GAS-Luc reporter) or HEK 293T cells (for ISRE-Luc and IFNβ-Luc) in 96-well plates were co-transfected with 75 ng of firefly luciferase reporter (GAS-Luc, ISRE-Luc or IFNβ-Luc), 10 ng of *TK-Renilla* plasmid and the desired expression plasmid using Trans-LT1 (Mirus Bio). In cases where different doses of the expression plasmids were used, the lower doses were topped up by addition of EV plasmids so that equal amounts of DNA were transfected per well. Twenty-four h post transfection, cells were either non-stimulated, or stimulated with IFNα (1000 U/mL, Sigma-Aldrich), IFNγ (25 ng/mL, PreproTech) or SeV (a gift from Steve Goodbourn) for 6, 8 or 24 h, respectively. Following stimulation, cells were lysed in passive lysis buffer (Promega) and firefly and *Renilla* luciferase luminescence were measured using a FLUOstar luminometer (BMG). Firefly values were normalised to *Renilla* luciferase readings and fold inductions were calculated for each sample relative to their own non-stimulated values. Results are presented as individual data point without P values. Relative protein expression levels were determined by immunoblotting.

Immunofluorescence

For VACV infection, A549 cells were seeded onto sterile glass coverslips (Thickness no. 0.13-0.17 mm, diameter 19 mm, Thermo Fisher Scientific) in 12-well plates. Twenty-four h after seeding, cells were serum starved for 16 h prior to infection. Cell were infected at 10 pfu/cell and at 2 h p.i., cells were washed once in medium before being stimulated with IFNγ (25 ng/mL, PreproTech) for 30 min.

For transfection, HeLa cells were seeded onto sterile glass coverslips (Thickness no. 1.5, diameter 22 mm, Thermo Fisher Scientific) in 6 well plates. Twenty-four h after seeding, cells were transfected with 0.8 μg of expression plasmids using TransIT LT1 (Mirus Bio). Five h post transfection, medium on cells was replaced with serum-free medium to serum starve cells for 16 h. Cells were then either non-stimulated, stimulated with IFNα (1000 U/mL, Sigma-Alrich) or stimulated with IFNγ (25 ng/mL, Prepotech) for 1 h.

Following stimulation, cells were fixed in 8% (v/v) paraformaldehyde (PFA, Electron Microscopy Sciences) in 250 mM HEPES pH 7.5 for 5 min on ice followed by 25 min at RT. After fixation, cells were incubated for 5 min with 50 mM ammonium chloride in PBS to quench free aldehydes. Cells were permeabilised by incubating with ice-cold, 100 % methanol at -20 °C for 10 min. Cells were blocked in IF buffer (10 % v/v FBS in PBS) for 30 min before staining with primary antibodies for 1 h. After washing, coverslips were then stained with secondary antibodies (AlexPhore) diluted in IF buffer, supplemented with 5% (v/v) serum from primary antibody source animal for each secondary antibody for 30 mins. Coverslips were then mounted using Mowiol 4-88 containing 4',6-diamidino-2-phenylindole (DAPI) on to microscope slides (Menzel-Gläser). Slides were visualised with a LSM 780 inverted confocal microscope (Zesis) and images were processed using Image J (Schindelin et al., 2012).

RT-qPCR

A549 cells in 12-well plates were infected at 10 pfu/cell. At 2 h p.i. cells were washed once in medium before being stimulated with IFNγ (25 ng/mL, PreproTech) for 1 h. Following stimulation, RNA was harvested using Monarch Total RNA Miniprep Kit (NEB) according to

manufacturer's instructions including an optional on-column genomic DNA digestion step. RT-qPCR was performed using Luna Universal One-Step RT-qPCR Kit (NEB). Oligonucleotide primers (**Table S2**) targeting HRPT and IRF1 were designed using PrimerQuest Tool (IDT). RT-qPCRs were carried out using a real-time PCR system (Thermo Fisher Scientific) and fold-inductions of ISG levels were calculated using $2^{-\Delta\Delta Ct}$ taking mock non-stimulated readings as the basal level sample and HRPT as the control housekeeping gene.

Pulldowns

For infection, BS-C-1 cells or MEFs in T-25 flasks were infected at 10 pfu/cell with either vTAP-018 or vTAP-N1. For transfection, 2fTGH, U3A, U6A and HEK 293T cells in 10-cm dishes, were transfected using either TranIT LT1 (Mirus Bio) for 2fTGH, U6A and U3A cells or polyethylenimine (PEI, 2 µl of 1 mg/mL stock per µg of DNA, Polysciences) for HEK 293T cells. Prior to transfection, medium was replaced with DMEM supplemented with 2% FBS. At 12 h p.i. or 18 h after transfection, cells were lysed in Tris-based IP buffer (50 mM Tris pH 7.4, 150 mM NaCl, 0.5% (v/v) NP-40) supplemented with protease (cOmplete Mini, Roche) and phosphatase inhibitors (PhosSTOP, Roche). Cell lysates were incubated with rotation at 4 °C for 15 mins before being cleared by centrifugation (21,000 RCF). A fraction of cleared lysate was taken for input samples and the remaining lysate was incubated with 30 µl of one of the following affinity resins washed and equilibrated in IP buffer: (i) Strep-Tactin XP super flow (IBA) for pulldown of TAP-tagged proteins via Strep-tag II epitope; (ii) anti-FLAG M2 affinity gel (Sigma-Aldrich) for immunoprecipitation of either FLAG or TAP-tagged protein via the FLAG epitope. Samples were incubated with affinity resins at 4 °C with rotation for 1 h 30 min. Samples were washed three times in IP buffer and proteins were eluted from beads by addition

of 2X SDS-gel loading buffer. Subsequently, samples were analysed by either Nu-PAGE (Thermo Fisher Scientific) or SDS-PAGE followed by immunoblotting.

For pulldowns using proteins produced from a cell-free transcription and translation system, the TnT Sp6 High-Yield wheat germ protein expression system (Promega) was utilised according to manufacturer's instructions.

In vivo experiments

Female BALB/c mice 6-10 weeks old were anesthetized and infected intranasally (i.n.) with 10^3 pfu for measurement of weight change and pulmonary virus titres or 10^5 pfu for extraction of RNA and RT-qPCR experiments. A final inoculation volume of 20 µl (10 µl per nostril) was used with VACVs diluted in HBSS + 0.1% BSA to achieve the required dose. The actual dose administered was confirmed by plaque assay of the diluted virus inoculum.

For weight change experiments, mice were weighed daily. For virus titration experiments, lungs were collected at 3, 7 and 9 days p.i. and single-cell suspensions were prepared by chopping with scissors followed by collagenase I digestion (Worthington Biochemicals) for 60 mins at 37 ºC. Cells were disrupted by vigorous pipetting and suspensions were freeze-thawed three times to release virus and infectious virus titres were determined by plaque assay on TK^- 143B cells. For RT-qPCR experiments the upper lobes of lungs were removed and immediately placed in buffer RLT (Qiagen). Lungs were homogenized and RNA was isolated using Lysing Matrix S (1/8") metal beads (MPBio) and a FastPrep®-24 Instrument (MPBio). RNA was then purified using a Qiagen RNeasy Mini Kit (Qiagen). An on-column DNAse (Sigma-Aldrich) digestion was performed prior to RNA elution. cDNA was synthesised using the RT^2 First

Strand Kit (Qiagen) with ~ 1.2 g of RNA/sample. cDNA was then loaded onto an Antiviral Response qPCR array (Qiagen) or onto a separate plate for the analysis of IRF1 and IFNγ for which individual RT^2 qPCR primer assays (Qiagen) were obtained. RT-qPCRs were carried out using RT^2 SYBR Green ROX qPCR mastermix (Qiagen) and a real-time PCR system (Thermo Fisher Scientific) and fold-changes of genes were calculated by comparing Ct values of individual vΔ018-infected mice (n=4) to the Ct averages of v018-infected mice (n=3) using the $2^{-\Delta\Delta Ct}$ method. Fold changes of genes were normalised against 5 standard housekeeping genes included on the Antiviral Response qPCR array (Qiagen) or against 3 standard housekeeping genes (Actb, B2M and GAPDH, Qiagen) for analysis of IRF1 and IFNγ (Qiagen). Data analysis and significances were performed using manufacturer's software (GeneGlobe Data Analysis Centre, Qiagen).

Protein expression and purification

The purity of protein preparations was analysed by SDS-PAGE and subsequent Coomassie blue staining (**Figure S7**).

Full-length STAT1 and $STAT1^{136\text{-}684,\Delta183\text{-}190,H182A,E393A,E394A}$ expression plasmids were transformed into *E. coli* T7 Express cells (NEB) and plated overnight on LB agar supplemented with 100 µg/mL of ampicillin. The next day colonies of transformed cells were collected and used to inoculate 1 L (TB) medium supplemented with 100 µg/mL of ampicillin and were grown at 37 ºC in 2 L flasks until OD_{600} of 0.8-1.2. Cultures were cooled to 18 ºC and incubated overnight with 0.4 mM IPTG to induce protein expression. Cells were collected by centrifugation and resuspended in lysis buffer (25 mL of 50 mM Tris-HCl, pH 8.0, 300 mM NaCl, 20 mM imidazole, 1 mM AEBSF, 1 mM TCEP) and lysed by sonication. Cell lysates

967 were centrifugated at 40,000 RCF for 30 min and the cleared supernatant was loaded on a 3
968 mL Ni-NTA agarose resin (Cube Biotech) or on a 5mL HisTrap HP column (Cytiva). The
969 column matrix was washed with 10 column volumes (CV) of wash buffer (50 mM Tris-HCl,
970 pH 8.0, 300 mM NaCl, 20 mM imidazole, 1 mM TCEP). Proteins were eluted with 50 mM
971 Tris-HCl, pH 8.0, 300 mM NaCl, 200 mM imidazole, 1 mM TCEP into 2 mL fractions.
972 Fractions containing the proteins of interest were pooled. STAT1$^{136\text{-}684,\ \Delta 183\text{-}190,\ H182A,\ E393A,\ E394A}$
973 fractions were incubated with 100 µL of 2 mg/mL TEV protease (prepared in-house) overnight
974 at 4 ºC to remove the N-terminal His_6 affinity tag. STAT1 proteins were then diluted ten-fold
975 in heparin buffer A (20 mM Tris-HCl, pH 8.0, 1 mM EDTA) and loaded on a 5 mL HiTrap
976 Heparin HP column (Cytiva) equilibrated with the same buffer. The column matrix was washed
977 with 10 CV heparin buffer A, followed by elution with a 0-100% linear gradient of heparin
978 buffer B (20 mM Tris-HCl pH 8.0, 1 mM EDTA, 1 M NaCl). STAT1 and STAT1(core)$^{\Delta 183\text{-}190,\ EE}$
979 eluted at approximately 20% heparin buffer B. Fractions containing protein of interest
980 were supplemented with TCEP (1 mM final) and concentrated on a centrifugal filter (MWCO
981 30,000 Da, Amicon) to 2 mL, after which the proteins were loaded on a Superdex 200 16/600
982 GL (Cytiva) size exclusion chromatography (SEC) column equilibrated with 20 mM Tris-HCl
983 pH 8.0, 300 mM NaCl, 1 mM EDTA. SEC fractions corresponding to the later-eluting major
984 peak were pooled and supplemented with TCEP (1 mM final), concentrated to ~0.5 mM on a
985 centrifugal filter (MWCO 30 000 Da, Amicon) and flash-frozen in liquid nitrogen.
986
987 GB1-018 and GB1-NiV-V fusions were expressed from pPEPT1 plasmids (TP, unpublished)
988 that were transformed into *E. coli* T7 Express cells (NEB) and plated overnight on LB agar
989 supplemented with 100 µg/mL of ampicillin. The next day transformed cells were collected
990 and used to inoculate 1 L TB medium supplemented with 100 µg/mL of ampicillin and were
991 grown at 37 ºC in 2 L flasks until OD_{600} of 0.8-1.2. Protein expression was induced with 0.4

mM IPTG for 3 h at 37 ºC. Following bacterial expression, a nickel affinity purification step was performed as described for STAT1 proteins. Fractions containing protein of interest were concentrated on a centrifugal filter (Amicon, MWCO 3000 Da) to 2 mL, after which the proteins were loaded on a Superdex 75 or Superdex 200 16/600 GL (Cytiva) SEC columns equilibrated with 20 mM Tris-HCl pH 8.0, 300 mM NaCl, 1 mM EDTA. SEC fractions corresponding to GB1 fusions were pooled, concentrated on a centrifugal filter (MWCO 3000 Da, Amicon) and flash-frozen in liquid nitrogen. For the purification of NiV-V proteins, buffers were supplemented with TCEP (1 mM final) to maintain cysteines in a reduced state.

Isothermal titration calorimetry (ITC)

All proteins were buffer-exchanged into ITC buffer (50 mM Tris-HCl pH 8.0, 150 mM NaCl, 1 mM EDTA, 0.1% Tween-20) using a NAP-5 size-exclusion column (Cytiva) and concentrations were determined by UV/Vis spectrophotometry and adjusted as needed. For measurements with synthetic peptides, peptides were re-suspended from lyophilised powder in MilliQ water and then concentrations were measured by UV-Vis and were adjusted to 10x the final value. Thereafter, the peptides were diluted ten-fold in ITC buffer. ITC measurements were performed on a Microcal ITC200 instrument (GE Healthcare) with 18 x 2 µL injections, 160 s interval and 5 µCal s^{-1} reference power. Baseline correction was performed using injection heats from protein-into-buffer runs. Integration of thermogram peaks and fitting of data was done using the Malvern ITC package in Origin 7.0 (Originlab). Isotherm fitting was performed using a one site model. All of the reaction conditions and fitted parameters are shown in **Table S5**.

Fluorescence polarisation (FP) anisotropy measurements

All proteins were buffer-exchanged into FP buffer (50 mM Tris pH 8.0, 300 mM NaCl, 1mM EDTA, 0.1% Tween-20, 1 mM TCEP) using a NAP-5 size-exclusion column (Cytiva) and concentrations were determined by UV/Vis spectrophotometry and adjusted as needed, after which, BSA was added to 0.1%. Fluorescein-conjugated pIFNGR1 12-mer peptide probe (Fluor-pIFNGR1) was first re-suspended in DMSO to 10 mM and then diluted in FP buffer plus 0.1% BSA to the required concentration. Reactions (40 µ) were set up in a 384-well non-transparent microplate (Corning, #3542). Competition reactions were performed with 10 nM Fluor-pIFNGR1 and fixed STAT1 concentration of 1.5 µM and two-fold serial dilutions of 018 or NiV-V GB1 fusions. Each dilution was measured in triplicate. Graphs show means ± SD (n=3) per dilution.

Measurements were performed on a Pherastar FS plate reader (BMG) using a FP 485/520/520 optical module. Reactions containing only 10 nM Fluor-pIFNGR1 were prepared as reference standards and were used to calibrate gain and focal height. Dose-response curves were fitted in Prism 9.0.0 (GraphPad) using a four-parameter logistic regression.

Peptides for ITC and FP

A 5-mer sequence (pYDKPH) of the pIFNGR1 is responsible for the vast majority of the receptor STAT1 SH2 domain interaction. For the FP assay we utilised a 12-mer peptide (5Flu-GTSFGpYDKPHVLV-NH2, PeptideSynthetics, UK) where TSFGpYDKPHVLV corresponds to 12 aa from pIFNGR1 and 5Flu-G represents an N-terminal 5-carboxyfluorescein and a spacer glycine. For our ITC measurement we utilised the 5-mer peptide (Ac-pYDKPH-NH2, Genosphere Biotechnologies) due to greater solubility compared to the 12-mer peptide.

Peptides were prepared using Fmoc-based solid-phase synthesis and purity was >95% as determined by HPLC.

SEC-MALS

SEC-MALS was performed using a Superdex 200 Increase 10/300 column (Cytiva) equilibrated with 50 mM Tris pH 8.0, 300 mM NaCl, 1 mM EDTA, 1 mM TCEP. The column was connected to a DAWN HELEOS II light scattering detector (Wyatt Technology) and the Optilab T-rEX refractive index detector (Wyatt Technology). Scattering was detected at 664 nm wavelength at RT. One hundred µL of sample was applied at a concentration of 20 µM for STAT1 and 100 µM of GB1-018. The experimental data were recorded and processed using the ASTRA software (Wyatt Technology).

X-ray crystallography

A STAT1 core fragment crystallography construct ($STAT1^{136\text{-}684,\Delta183\text{-}190,H182A,E393A,E394A}$) was prepared harbouring a loop deletion at the apex of the coiled coil domain (Δ183-190,H182A) and surface entropy-reducing mutations (E393A,E394A). The STAT1-018 complex was co-crystallised using sitting-drop vapour diffusion in a 96-well MRC plate format. The complex was prepared by mixing $STAT1^{136\text{-}684,\Delta183\text{-}190,H182A,E393A,E394A}$ in SEC buffer (20 mM Tris-HCl pH 8.0, 300 mM NaCl, 1 mM EDTA) and 018 21-mer peptide (Ac-MWSVFIHGHDGSNKGSKTYTS-NH2, Genosphere Biotechnologies) in 20 mM Tris-HCl pH 8.0, to a final concentration of 5 mg/mL protein and 2 mg/mL peptide. Three hundred nL of the complex was mixed with 300 nL of the crystallisation condition using a Mosquito liquid handling robot (TTP Labtech). Crystals were obtained using the following condition: 16% PEG 3350, 175 mM KCl, 125 mM $(NH_4)_2SO_4$. Cryoprotectant solution containing the crystallisation

condition and 30% ethylene glycol was added to the drop and crystals were incubated for 1 min. A crystal was then harvested and cryo-cooled in liquid nitrogen. Diffraction data were collected at Diamond Light Source (Harwell, UK) synchrotron radiation source, beamline i04. Diffraction images were processed with autoPROC (Vonrhein et al., 2011). Molecular replacement phasing was used with STAT1 core residues 133-683 (PDB ID: 1YVL) as a search model. The structure was refined without peptide first and the peptide was built into the clearly visible electron density manually **(Figure S6A)**. Manual real-space refinement was done in Coot (Emsley et al., 2010) and automated refinement with phenix.refine (Liebschner et al., 2019) and autoBUSTER (Smart et al., 2012). Crystallographic data and refinement statistics are shown in **Table S4**. The coordinates and corresponding structure factors have been deposited to the PDB under accession number PDB: 7nuf.

Supplemental information

Plasmid	Primers 5'-3'
pcDNA4/TO TAP-018	AAA**GCGGCCGC**GATGAGTTCTAAAGGCGGATCTTC
	AAA**TCTAGA**TTAGATTTTGCCGGTGCCGC
pcDNA/TO TAP-NiV-V	AAAA**GCGGCCG**CGGATAAATTGGAACTAGTCAA
	AAAA**TCTAGA**TTAACCGCAGTGGAAGCATTCAG
pcDNA4/TO TAP-018 (1-54)	AAA**GCGGCCGC**GATGAGTTCTA
	AAA**TCTAGA**TTATTTCACGCCGCCGTTCACGC
pcDNA4/TO TAP-018 (1-48)	AAA**GCGGCCGC**GATGAGTTCTA
	AAA**TCTAGA**TTAGCCAGACTTCACTCCGCTA
pcDNA4/TO TAP-018 (1-43)	AAA**GCGGCCGC**GATGAGTTCTA
	AAA**TCTAGA**TTAGCTAGATGATCCTCCGCCCCA
pcDNA4/TO TAP-018 (1-35)	AAA**GCGGCCGC**GATGAGTTCTA
	AAA**TCTAGA**TTATCCTCCGCCGCCAGATGT
pcDNA4/TO TAP-018 (1-30)	AAA**GCGGCCGC**GATGAGTTCTA
	AAA**TCTAGA**TTATGTGTATGTCTTGCTGCCCT
pcDNA4/TO TAP-018 (1-27)	AAA**GCGGCCGC**GATGAGTTCTA
	AAA**TCTAGA**TTACTTGCTGCCCTTGTTGCTG
pcDNA4/TO TAP-018 (1-24)	AAA**GCGGCCGC**GATGAGTTCTA
	AAA**TCTAGA**TTACTTGTTGCTGCCATCGTGG
pcDNA4/TO TAP-018 (1-21)	AAA**GCGGCCGC**GATGAGTTCTA
	AAA**TCTAGA**TTAGCCATCGTGGCCGTGGAT
pcDNA4/TO TAP-018 (8-60)	AAA**GCGGCCGC**GTCTGGCGGCATGTGGAGC
	AAA**TCTAGA**TTAGATTTTGCCGGTGCCGCTT
pcDNA4/TO TAP-018 (11-60)	AAA**GCGGCCGC**GATGTGGAGCGTGTTCATCCA
	AAA**TCTAGA**TTAGATTTTGCCGGTGCCGCTT
pcDNA4/TO TAP-018 (14-60)	AAA**GCGGCCGC**GGTGTTCATCCACGGCCACG
	AAA**TCTAGA**TTAGATTTTGCCGGTGCCGCTT
pcDNA4/TO TAP-018 (17-60)	AAA**GCGGCCGC**GCACGGCCACGATGGCAG
	AAA**TCTAGA**TTAGATTTTGCCGGTGCCGCTT
pcDNA4/TO TAP-018 (22-60)	AAA**GCGGCCGC**GAGCAACAAGGGCAGCAAGAC
	AAA**TCTAGA**TTAGATTTTGCCGGTGCCGCTT
pcDNA4/TO TAP-018 (31-60)	AAA**GCGGCCGC**GTCTGGCGGCGGAGGAATGT
	AAA**TCTAGA**TTAGATTTTGCCGGTGCCGCTT
pcDNA4/TO TAP-018^{KDA}	CGCCGATGGCAGCAACAAGGG*
	CCGGCGATGAACACGCTCCACATG*
pcDNA3 HA-018	SUBCLONED FROM PCDNA4/TO NTAP-018
pcDNA3 HA-018^{KDA}	CGCCGATGGCAGCAACAAGGG*
	CCGGCGATGAACACGCTCCACATG*
pcDNA3 V5-STAT1	AAAA**GCGGCCGC**GTCTCAGTGGTACGAACTTCA
	AAAA**GGGCCC**TTATACTGTGTTCATCATAC
pcDNA3 V5-STAT2	AAA**GCGGCCGC**GATGGCGCAGTGGGAAATGCT
	AAA**CTCGAG**TTAGAAGTCAGAAGGCATCAAG
pcDNA3 V5-STAT3 (human)	AAA**GCGGCCGC**GATGGCCCAATGGAATCAGCT
	AAA**CTCGAG**TTACATGGGGGAGGTAGCGC
pcDNA3 V5-STAT3 (mouse)	AAA**GCGGCCGC**GGCTCAGTGGAACCAGCTGCA
	AAA**GGGCCC**TCACATGGGGGAGGTAGCAC
pcDNA3 V5-STAT4	AAA**GCGGCCGC**GATGTCTCAGTGGAATCAAGTCC
	AAA**CTCGAG**TTATTCAGCAGAATAAGGAGACTTC
pcDNA3 V5-STAT5A	AAA**GCGGCCGC**GATGGCGGGCTGGATCCA
	AAA**CTCGAG**TTATGAGAGGGAGCCTCTGGC
pcDNA3 V5-STAT5B	AAA**GCGGCCGC**GATGGCTGTGTGGATACAAGCTCA
	AAA**CTCGAG**TTACGATTGTGCGTGCGGGA
pcDNA3 V5-STAT6	AAA**GCGGCCGC**GATGTCTCTGTGGGGTCTGGTC
	AAA**CTCGAG**TTACCAACTGGGGTTGGCCCT
pcDNA3 V5-STAT1 (1-712)	AAAA**GCGGCCGC**GTCTCAGTGGTACGAACTTCA
	AAAA**GGGCCC**TTAAACTTCAGACACAGAAATCAA
pcDNA3 V5-STAT1 (1-684)	AAAA**GCGGCCGC**GTCTCAGTGGTACGAACTTCA
	AAAA**GGGCCC**TTATGGCCTGGAGTAATACTTTC
pcDNA3 V5-Fus1	AAAA**GCGGCCGC**GGCTCAGTGGAACCAGCTGCA
	*CCCTTCATTCCAAAG*GGCCAAG
	*CTTTGGAATGAAGGG*TGCATCATGGGCTTCAT
	AAAA**GGGCCC**TTATACTGTGTTCATCATAC
pcDNA3 V5-Fus2	AAAA**GCGGCCGC**GTCTCAGTGGTACGAAC
	CCCATCATTCCAGAGAGGGA
	*TCCCTCTCTGGAATGATGGG*TACATCATGGGTTTCATCAG
	AAAA**GGGCCC**TTACATGGGGGAGGTAGCACAC
pcDNA3 V5-STAT3^{S663H} (Human)	GACCCAGATCCACTCCGTGGAAC*
	TTACCGCTGATGTCCTTC*
pF3A TAP-018	AAA**GATCG**ATGTGGTCTCATCCTCAGTT
	AAA**GTTTAAAC**TTAGATTTTGCCGGTGCCGC
pF3A STAT1	AAA**GATCG**ATGTCTCAGTGGTACGAACTTCA
	AAA**GTTTAAAC**TTATACTGTGTTCATCATAC
pUC13-Ecogpt-EGFP Δ018	AAA**CTGCAG**TGCCACTGTCTAGTAGTAGT
	AAA*GCGGCCGCATACTCGAG*ACACTAAATTATTTTTATTA
	AAA*CTCGAGTATGCGGCCGC*ATTAATAAGACTTAAGGACA
	AAA**GGATCC**CTAATAAGTTAATAGAACAA
pUC13-Ecogpt-EGFP TAP-018	AAA**TCTAGA**TGCCACTGTCTAGTAGTAGT.
	AAA**GCGGCCGC**GATGTCTTCTAAAGGGGGTA
	ATTAATAAGACTTAAGGACA.
	AAA**GGATCC**GCTAATAAGTTAATAGAACAA.
	AAA**CTGCAG**TGCCACTGTCTAGTAGTAGT.
	*TGTCCTTAAGTCTTATTAATA*TGTGGTCTCATCCTCAGTT
pOPTH_TEV	CCGGAGAGCTCCAATTGGA.
	AAA**GGATCC**CTGGAAGTACAGGTTTTCGGTACCGCTATGGTGATGGTGATGATGAG CCAT
pOPTH_TEV STAT1$^{136-684,\Delta183-190,H182A,E393A,E394A}$	AAA**GGATCC**ACAGTGATGTTAGACAAACAG
	AAA**ACGCGT**TTATGGCCTGGAGTAATACTTT
	*TTGCAGAACAGAGAAGC*GGATCAGAAACAAGAACAGCTGTTACTC
	*TTCTCTGTTCTGCAAG*GTTTTG
	GATGAACATGGCGGCGTCCACCAATG*
	ACTTTTGTGTGCGTGCCC*
pEXP-nHis-STAT1-cStrep	GAAAACCTGTACTTCCAGGGTTCTCAGTGGTACGAACTTCAGCAG
	GCTCCATGCGCTCGATACTGTGTTCATCATACTGTCGAATTC
pPEPT 018	GGAA**GGATCC**GGCGGCATGAGTTCTAAAGGCGGATC
	AAA**CTCGAG**CCGATTTTGCCGGTGCCGCTTTTC
pPEPT 018^{T2}	GGAA**GGATCC**GGCGGCATGTGGAGCGT
	AAA**CTCGAG**CCAGATGTGTATGTCTTGCTGCCC
pPEPT 018^{T3}	GGAA**GGATCC**GGCGGCATGTGGAGCGT
	AAA**CTCGAG**CCCTTGCTGCCCTTGTTGCTG
pPEPT 018^{KDA}	CGCCGATGGCAGCAACAAGGG*
	CCGGCGATGAACACGCTCCACATG*
pPEPT-NiV-V (110-140)	AAA**GGATCC**GGCGGCGTGGTTACAGACGTTGTATA
	AAA**CTCGAG**CCTGTGTAATCACTCCACCCTC
pPEPT-NiV-V (110-140)^{KDA}	TGCTGGAGGAGAATGTACCGGA*
	TCAGCGTATACAACGTCTGTAACCAC*

Table S1. Oligonucleotide primers for construction of recombinant DNA. Related to STAR methods

Cloning sites are highlighted in bold (for restriction digest cloning) or underlined (for ligation-independent cloning). Complementary sequences for overlapping PCR are italicised. Site-directed mutagenesis primers are indicated with an asterisk (*). All V5 and TAP-tagged proteins are tagged at the N terminus.

Target Gene	Primers 5'-3'
HRPT	CGAGATGTGATGAAGGAGATGG
	TTGATGTAATCCAGCAGGTCAG
IRF1	CATTCACACAGGCCGATACA
	TGGTCTTTCACCTCCTCGATA

1084

1085 **Table S2. Oligonucleotide primers for RT-qPCR. Related to STAR methods.**

1086

Target	Primers 5-3'
STAT1 Internal	ATGCTTGCTTGGATCAGC
STAT2 Internal	GTTGGAACAGCTGGAGAC
STAT3 (human) Internal	CAACTTCAGACCCGTCAAC
STAT4 Internal	GAGCTGCAAGACTGGAA
STAT5A Internal	GATGACGAGCTGATCCAGTG
STAT5B Internal	GACGAGCTGATCCAGTGG
STAT6 Internal	GCTGGATGAAGTCCTGAG
VACWR018 Upstream	GTGAACTCTATACACCCACAC
VACWR018 Downstream	ACATTTGATTTTCTCGTACGC

1087

1088 **Table S3. Oligonucleotide primers for analytical PCR or sequencing. Related to STAR**

1089 **methods.**

PDB ID: 7nuf

Data collection and processing	
Wavelength (Å)	0.9795
Space group	C 1 2 1
Data collection temperature (K)	100
a, b, c (Å)	169.06, 37.47, 115.48
α, β, γ (°)	90.00, 116.19, 90.00
Resolution range (high resolution bin) (Å)	80.42 - 2.00 (2.00 - 2.04)
R_{meas}	0.124 (3.251)
Completeness (%)	99.7 (99.8)
Number of total / unique reflections	183215 / 44523
Redundancy	4.1 (4.3)
$\langle I/\sigma(I)\rangle$	6.6 (0.5)
$CC_{1/2}$	1.0 (0.4)
Refinement	
R_{cryst} /R_{free}	0.224 / 0.256
Number of reflections in test set	2136
Number of atoms	4659
Mean/Wilson B-factor (Å^2)	61 / 44.3
Ramachandran favoured/allowed/outliers (%)	98.86/ 1.14 / 0
RMSD bonds (Å)	0.009
RMSD angles (°)	1.309

Table S4. X-ray crystallographic data collection and refinement statistics.

Reaction	Cell	Syringe	K_d, nM	N	ΔH, cal / mol	ΔS, cal / mol / deg
018 + STAT1	10 μM STAT1	100 μM 018	291	1.02	-1.93 x 10^4	-34.9
018T2 + STAT1	15 μM STAT1	150 μM 018T2	235	1.01	-1.87 x 10^4	-32.3
018T3 + STAT1	15 μM STAT1	350 μM 018T3	>10^4	1.00 (fixed)	-2.01 x 10^4	-46.8
018AGA + STAT1	10 μM STAT1	100 μM 018AGA	No binding	n.a.	n.a.	n.a.
pIFNGR1 + STAT1	10 μM STAT1	300 μM pIFNGR1 5-mer	7.6 x 10^3	0.708	-9172	-7.33
pIFNGR1 + STAT1 / 018	10 μM STAT1 + 50 μM 018	300 μM pIFNGR1 5-mer	No binding	n.a.	n.a.	n.a.
pIFNGR1 + STAT1 / 018 AGA	10 μM STAT1 + 50 μM 018 AGA	300 μM pIFNGR1 5-mer	7.8 x 10^3	0.79	-8001	-3.48
pIFNGR1 + STAT1 / NiV-V	10 μM STAT1 + 200 μM Ni V	300 μM pIFNGR1 5-mer	No binding	n.a.	n.a.	n.a.
pIFNGR1 + STAT1 / NiV-V ADA	10 μM STAT1 + 200 μM Ni V ADA	300 μM pIFNGR1 5-mer	7.2 x 10^3	0.88	-8125	-3.72

Table S5. ITC experimental conditions and fitted parameters

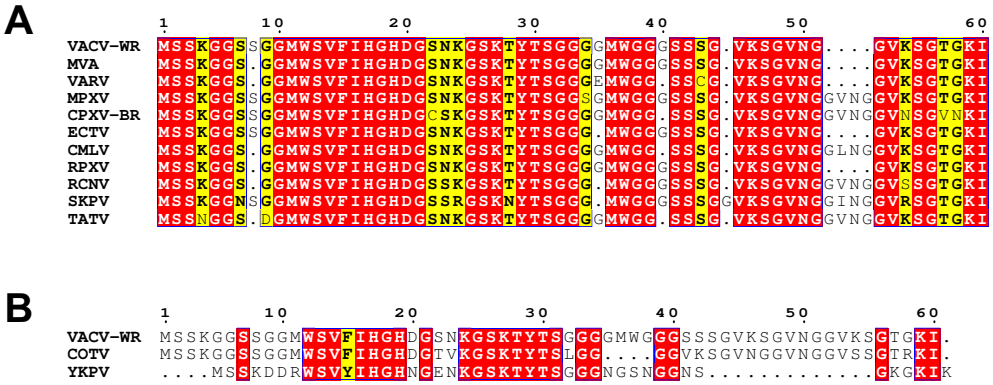

Figure S1. Sequence alignment of 018 orthologues.

(**A**) Alignment of 018 orthologues from representative orthopoxviruses: vaccinia strain Western Reserve (VACV-WR), modified vaccinia Ankara (MVA), variola virus (VARV), monkeypox virus (MPXV), cowpox virus strain Brighton Red (CPXV), ectromelia virus (ECTV), camelpox virus (CMPV), rabbitpox virus (RPXV), racconpox virus (RCNV),

skunxpox virus (SKPV) and taterpox virus (TATV). The 018 ORF is absent from VACV strain Copenhagen. (**B**) Alignment of 018 poxvirus orthologues from Cotia virus (COTV) and yokapoxvirus (YKPV), which sit outside of the orthopoxvirus genus. Identical residues are shown in red, similar residues are shown in yellow (**A-B**).

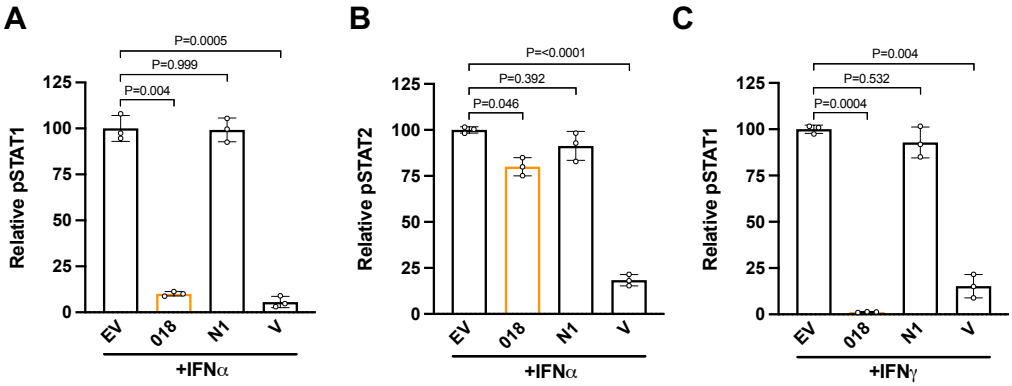

Figure S2. Related to Figure 2

Quantification of relative band intensities (**Figure 2**) for pSTAT1 **(A)** and pSTAT2 (**B**) from (**Figure 2C)** and pSTAT1 **(C)** from (**Figure 2D**). pSTAT levels were normalised against total STAT levels and made relative to EV condition. Means ± SD (n=3 per condition) are shown. Significances were calculated by Dunnett's T3 multiple comparisons test.

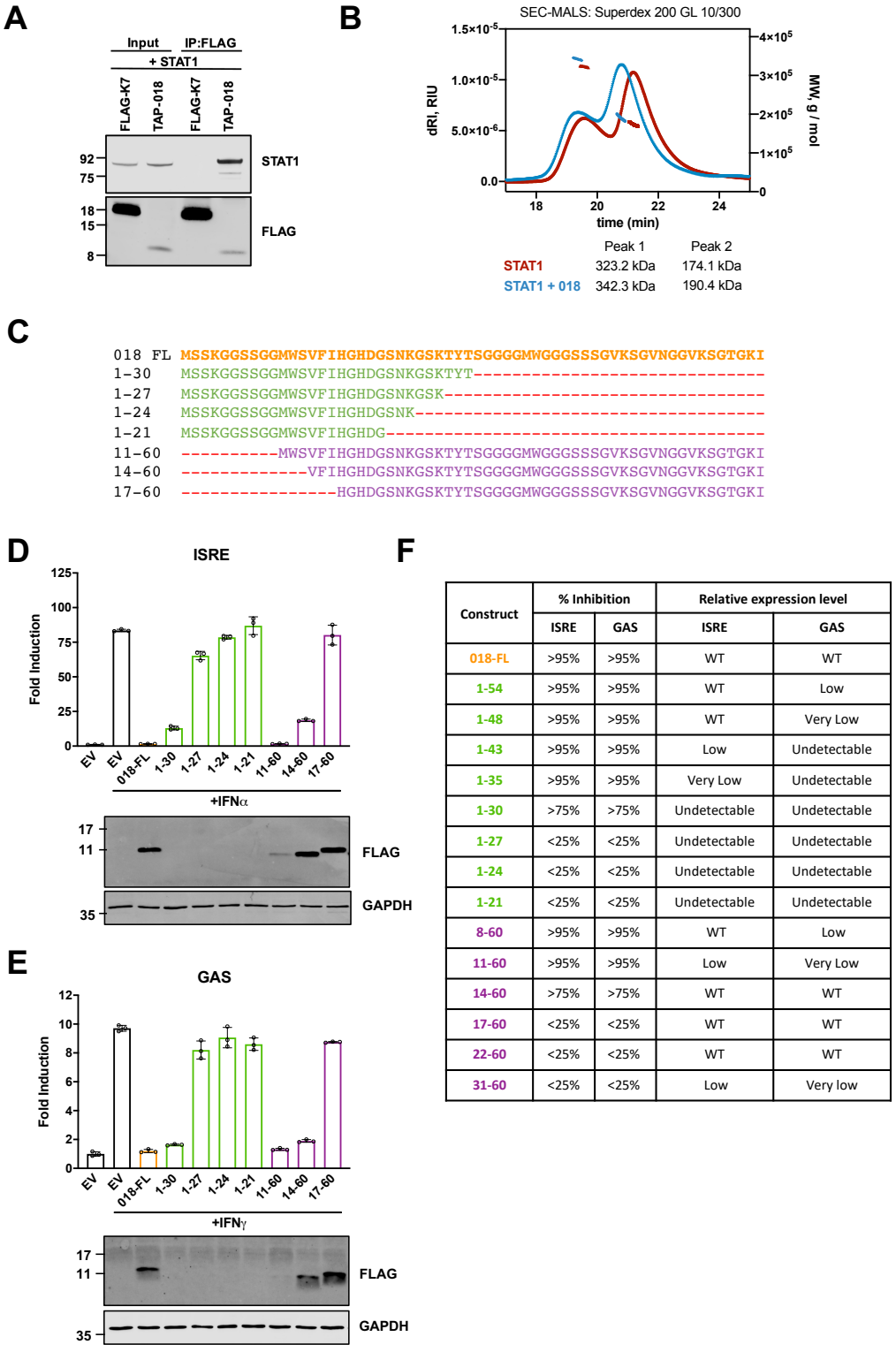

Construct	% Inhibition		Relative expression level	
	ISRE	GAS	ISRE	GAS
018-FL	>95%	>95%	WT	WT
1-54	>95%	>95%	WT	Low
1-48	>95%	>95%	WT	Very Low
1-43	>95%	>95%	Low	Undetectable
1-35	>95%	>95%	Very Low	Undetectable
1-30	>75%	>75%	Undetectable	Undetectable
1-27	<25%	<25%	Undetectable	Undetectable
1-24	<25%	<25%	Undetectable	Undetectable
1-21	<25%	<25%	Undetectable	Undetectable
8-60	>95%	>95%	WT	Low
11-60	>95%	>95%	Low	Very Low
14-60	>75%	>75%	WT	WT
17-60	<25%	<25%	WT	WT
22-60	<25%	<25%	WT	WT
31-60	<25%	<25%	Low	Very low

Figure S3. Related to Figure 3

(**A**) 018:STAT1 interaction using a cell-free transcriptional and translation system. Untagged-STAT1 was co-expressed along with either FLAG-tagged K7 or TAP-tagged 018 using a wheat

germ cell free transcriptional and translation system. FLAG-K7 and TAP-018 were precipitated using M2-FLAG affinity gel and purified proteins were analysed by immunoblotting with α-FLAG and α-STAT1 antibodies. (**B**) SEC-MALS measurements of purified free STAT1 (red) and STAT1:GB1-018 complex (blue). One hundred µl samples were loaded on a Superdex 200 GL 10/300 column and scattering and refractive index of the eluting peaks were measured. Concentration of 20 µM for STAT1 and 100 µM of GB1-018 were applied. (**C**) Sequences for C-terminal (green) and N-terminal (purple) 018 refined truncation mutants. (**D**) HEK 293T cells or (**E**) HeLa cells were transfected with reporter plasmids ISRE-Luc (**D**) or GAS-Luc (**E**) plus *TK-Renilla* and vectors expressing 018 truncation mutants from (**C**) fused to a TAP-tag. Cells were stimulated with IFNα (1000 U/mL) (**D**), or IFNγ (25 ng/mL) (**E**) for 6 h (**D**) or 8 h (**E**) and luciferase values were measured. Means ± SD (n=3 per condition) are shown. Lysates were prepared and analysed by immunoblotting with α-FLAG and α-GAPDH. (**F**) Summary table of all C-terminal (green) and N-terminal (purple) 018 truncation mutants describing the percentage inhibitory activity (>95%, >75% (but less then >95%) or <25%) and relative protein expression levels (wild type (WT), low, very low or undetectable) for ISRE (IFNα) and GAS (IFNγ) reporters. Data from (**D-E**) are representative of 2 individual experiments.

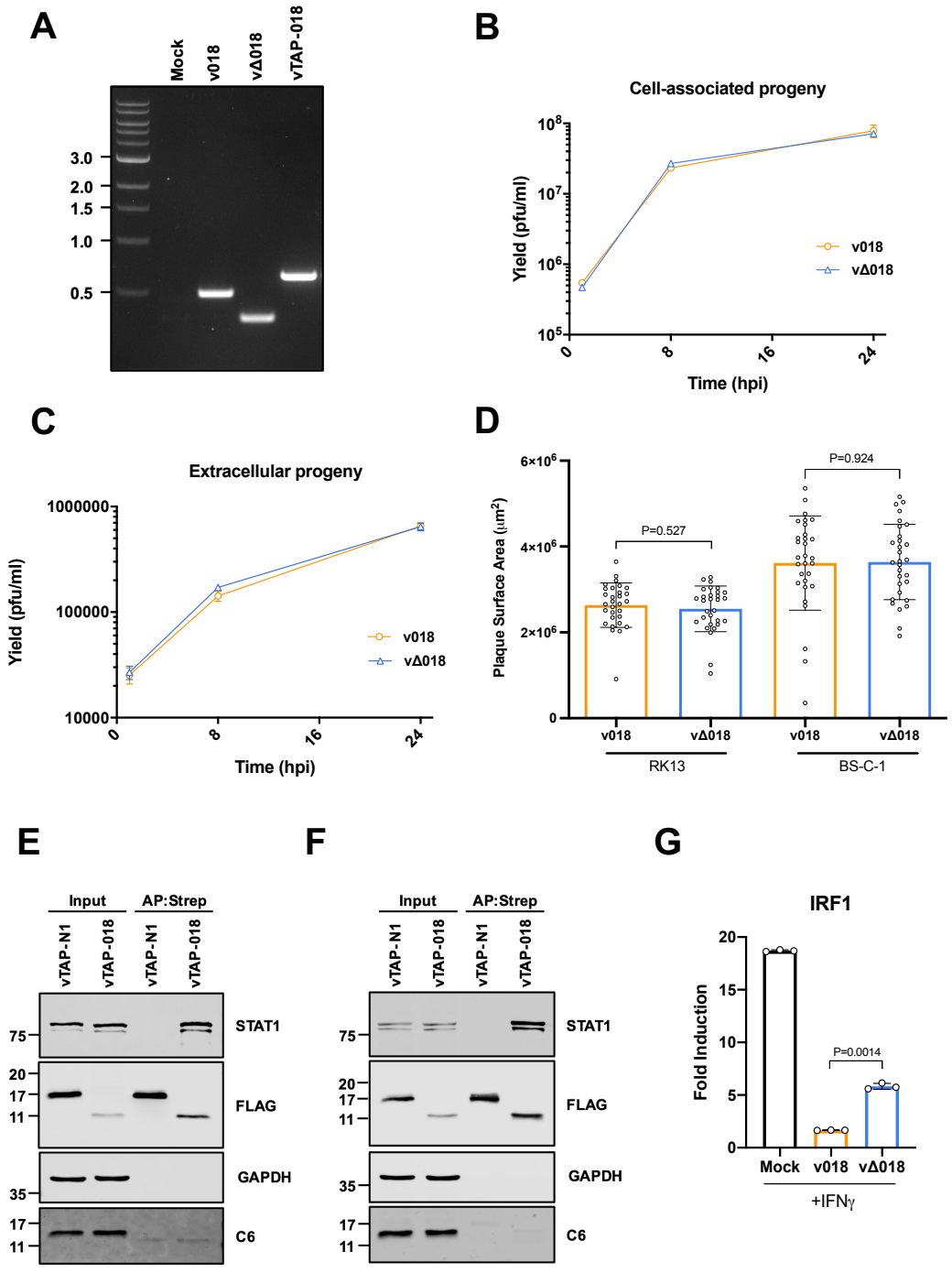

Figure S4. Related to Figure 4

(**A**) PCR amplification of genomic DNA from the indicated viruses using primers upstream and downstream of the 018 ORF. The position of DNA size markers (kb) are shown on the left side of the image. (**B, C**) BS-C-1 cells were infected with either v018 (orange) or vΔ018 (blue) at 5 pfu/cell. At 1, 8 and 24 h p.i. infectious virus titres associated with cells (**B**) and in the

supernatants (**C**) was determined by plaque assay on BS-C-1 cells. Means ± SD (n=2 per condition) are shown and P=>0.05 for all timepoints. **(D)** RK13 or BS-C-1 cells were infected at 30 pfu per well with either v018 (orange) or vΔ018 (blue). At 72 h p.i. monolayers were stained and plaque surface areas were quantified. Means ± SD (n=30 plaques per condition) are shown. **(E)** BS-C-1 cells or **(F)** MEFs were infected with vTAP-018 or vTAP-N1 at 5 pfu/cell for 12 h. TAP-tagged proteins were affinity-purified by Strep-Tactin and whole cell lysates (Input) and affinity-purified proteins (AP:Strep) were analysed by immunoblotting with α-FLAG, α-GAPDH, α-STAT1 and α-C6. Data for (**B-F**) are representative of two individual experiments. (**G**) A549 cells were mock-infected or infected with v018 or vΔ018 at 10 pfu/cell. At 2 h p.i. cells were stimulated IFNγ (25 ng/mL) for 1 h. Total RNA was extracted and mRNA for IRF1 was analysed by RT-qPCR. Means ± SD (n=3 per condition) are shown. Data are representative of two individual repeats. Significances were determined using Unpaired t-test with Welch's correction (**B-D**, **G**).

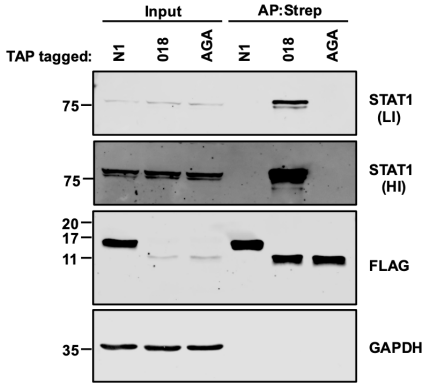

Figure S5. Related to Figure 6

TAP-tagged 018, 018 AGA (labeled AGA) and N1 were expressed by transfection in 2fTGH cells and affinity purified by Strep-Tactin. Whole cell lysates (Input) and affinity-purified

1159 proteins (AP:Strep) were analysed by immunoblotting with α-FLAG, α-GAPDH and α-

1160 STAT1. A high intensity (HI) and low intensity (LI) scan of α-STAT1 are shown.

1161

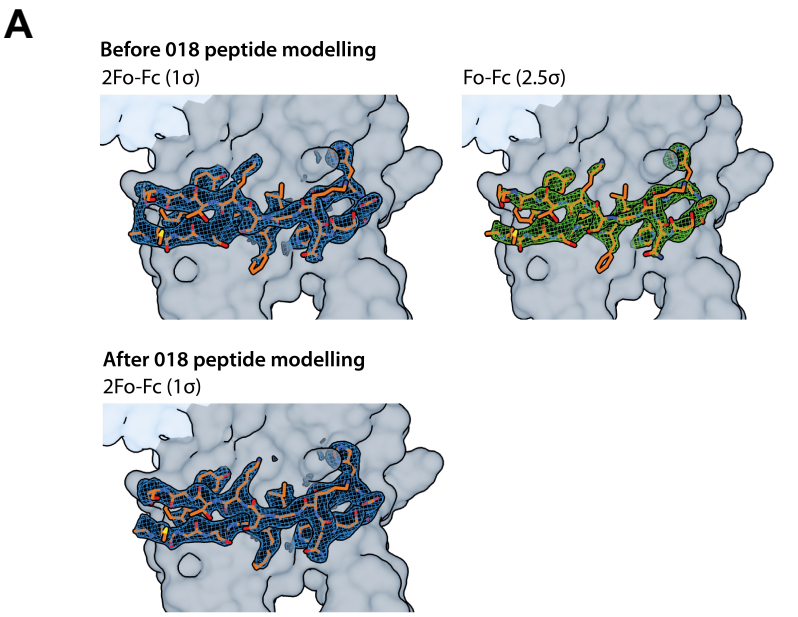

B

```
                                  K584  K588
STAT1   576 GCIMGFISKERERALLKDQQPGTFLLRFSESSSREGA 611
STAT2   575 GRIMGFVSRSQERRLLKKTMSGTFLLRFSESS  EGG 609
STAT3   583 GYIMGFISKERERAILSTKPPGTFLLRFSESSKEGG 618
STAT4   572 GYVMGFVSKEKERLLLKDKMPGTFLLRFSESH  LGG 606
STA5A   592 GAILGFVNKQQAHDLLINKPDGTFLLRFSDSE  IGG 626
STA5B   592 GAILGFVNKQQAHDLLINKPDGTFLLRFSDSE  IGG 626
STAT6   536 RLIIGFISKQYVTSLLLNEPDGTFLLRFSDSE  IGG 570

                                  H629
                            F628  A630 E632 Y634
STAT1   612 ITFTWVERSQNGGEPDFHAVEPYTKKELSAVTFPDI 647
STAT2   610 ITCSWVEHQDD DKVLIYSVQPYTKEVLQSLPLTEI 644
STAT3   619 VTFTWVEKDIS GKTQIQSVEPYTKQQLNNMSFAEI 653
STAT4   607 ITFTWVDHSES GEVRFHSVEPYNKGRLSALPFADI 641
STA5A   627 ITIAWKFD  S PERNLWNLKPFTTRDFSIRSLADR 659
STA5B   627 ITIAWKFD  S QERMFWNLMPFTTRDFSIRSLADR 659
STAT6   571 ITIAHVIRGQD GSPQIENIQPFSAKDLSIRSLGDR 605

            Y651 V653
STAT1   648 IRNYKVMAAENIPENPLKYLYPNIDKDHAFGKYYSR 683
STAT2   645 IRHYQLLTEENIPENPLRFLYPRIPRDEAFGCYYQE 680
STAT3   654 IMGYKIMDATNILVSPLVYLYPDIPKEEAFGKYCRP 689
STAT4   642 LRDYKVIMAENIPENPLKYLYPDIPKDKAFGKHYSS 677
STA5A   660 LGDL          SYLIYVFPDRPKDEVFSKYYTP 685
STA5B   660 LGDL          NYLIYVFPDRPKDEVYSKYYTP 685
STAT6   606 IRDL          AQLKNLYPKKPKDEAFRSHYKP 631
```

1162

1163 **Figure S6. Related to Figure 7**

1164 **(**A**)** Electron density maps of 018 peptide before and after peptide modelling and refinement.

1165 **(**B**)** Alignment of STAT family SH2 domains with residues that form contacts with 018 in the

1166 018:STAT1 crystal structure highlighted in orange.

1167

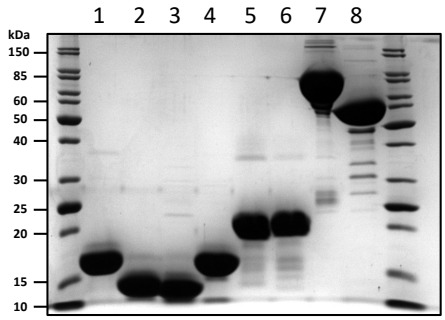

1. GB1-018 FL
2. GB1-018 FL
3. GB1-018 T3
4. GB1-018 AGA
5. NiV-V 110-140
6. NiV-V 110-140 ADA
7. STAT1 FL
8. STAT1 136-684,Δ183-190,H182A,E393A,E394A

1168

1169 **Figure S7. Coomassie-stained SDS-polyacrylamide gel of purified recombinant proteins.**

1170

1171

References

Aaronson, D.S., and Horvath, C.M. (2002). A road map for those who don't know JAK-STAT. Science. *296*, 1653–1655.

Albarnaz, J., Torres, A., and Smith, G. (2018). Modulating Vaccinia Virus Immunomodulators to Improve Immunological Memory. Viruses. *10*, 101.

Alcamí, A., and Smith, G.L. (1995). Vaccinia, cowpox, and camelpox viruses encode soluble gamma interferon receptors with novel broad species specificity. J. Virol. *69*, 4633–4639.

Alcamí, A., Symons, J.A., and Smith, G.L. (2000). The Vaccinia Virus Soluble Alpha/Beta Interferon (IFN) Receptor Binds to the Cell Surface and Protects Cells from the Antiviral Effects of IFN. J. Virol. *74*, 11230–11239.

Arunkumar, G., Chandni, R., Mourya, D.T., Singh, S.K., Sadanandan, R., Sudan, P., and Bhargava, B. (2019). Outbreak investigation of nipah virus disease in Kerala, India, 2018. J. Infect. Dis. *219*, 1867–1878.

Assarsson, E., Greenbaum, J.A., Sundström, M., Schaffer, L., Hammond, J.A., Pasquetto, V., Oseroff, C., Hendrickson, R.C., Lefkowitz, E.J., Tscharke, D.C., et al. (2008). Kinetic analysis of a complete poxvirus transcriptome reveals an immediate-early class of genes. Proc. Natl. Acad. Sci. USA. *105*, 2140–2145.

Bandi, P., Pagliaccetti, N.E., and Robek, M.D. (2010). Inhibition of type III interferon activity by orthopoxvirus immunomodulatory proteins. J. Interf. Cytokine Res. *30*, 123–133.

Bartlett, N.W., Buttigieg, K., Kotenko, S. V., and Smith, G.L. (2005). Murine interferon lambdas (type III interferons) exhibit potent antiviral activity in vivo in a poxvirus infection model. J. Gen. Virol. *86*, 1589–1596.

Bateman, A. (2019). UniProt: A worldwide hub of protein knowledge. Nucleic Acids Res. *47*, D506–D515.

1196 Briscoe, J., Rogers, N.C., Witthuhn, B.A., Watling, D., Harpur, A.G., Wilks, A.F., Stark, G.R.,
1197 Ihle, J.N., and Kerr, I.M. (1996). Kinase-negative mutants of JAK1 can sustain interferon-
1198 gamma-inducible gene expression but not an antiviral state. EMBO J. *15*, 799–809.
1199 Chiuppesi, F., Salazar, M. d'Alincourt, Contreras, H., Nguyen, V.H., Martinez, J., Park, Y.,
1200 Nguyen, J., Kha, M., Iniguez, A., Zhou, Q., et al. (2020). Development of a multi-antigenic
1201 SARS-CoV-2 vaccine candidate using a synthetic poxvirus platform. Nat. Commun. *11*, 1–16.
1202 Chua, K.B. (2000). Nipah Virus: A Recently Emergent Deadly Paramyxovirus. Science. *288*,
1203 1432–1435.
1204 Ciancanelli, M.J., Volchkova, V.A., Shaw, M.L., Volchkov, V.E., and Basler, C.F. (2009).
1205 Nipah Virus Sequesters Inactive STAT1 in the Nucleus via a P Gene-Encoded Mechanism. J.
1206 Virol. *83*, 7828–7841.
1207 Colamonici, O.R., Domanski, P., Sweitzer, S.M., Larner, A., and Buller, R.M.L. (1995).
1208 Vaccinia virus B18R gene encodes a type I interferon-binding protein that blocks interferon α
1209 transmembrane signaling. J. Biol. Chem. *270*, 15974–15978.
1210 Davey, N.E., Travé, G., and Gibson, T.J. (2011). How viruses hijack cell regulation. Trends
1211 Biochem. Sci. *36*, 159–169.
1212 Dyer, M.D., Murali, T.M., and Sobral, B.W. (2008). The landscape of human proteins
1213 interacting with viruses and other pathogens. PLoS Pathog. *4*, e32.
1214 Elde, N.C., and Malik, H.S. (2009). The evolutionary conundrum of pathogen mimicry. Nat.
1215 Rev. Microbiol. *7*, 787–797.
1216 Emsley, P., Lohkamp, B., Scott, W.G., and Cowtan, K. (2010). Features and development of
1217 Coot. Acta Crystallogr. Sect. D Biol. Crystallogr. *66*, 486–501.
1218 Falkner, F.G., and Moss, B. (1990). Transient dominant selection of recombinant vaccinia
1219 viruses. J. Virol. *64*, 3108–3111.
1220 García-Arriaza, J., Garaigorta, U., Pérez, P., Lázaro-Frías, A., Zamora, C., Gastaminza, P., del

1221 Fresno, C., Casasnovas, J.M., S. Sorzano, C.Ó., Sancho, D., et al. (2021). COVID-19 Vaccine
1222 Candidates Based on Modified Vaccinia Virus Ankara Expressing the SARS-CoV-2 Spike
1223 Protein Induce Robust T- and B-Cell Immune Responses and Full Efficacy in Mice. J. Virol.
1224 *95*. e02260-20
1225 García-Sastre, A. (2017). Ten Strategies of Interferon Evasion by Viruses. Cell Host Microbe.
1226 *22*, 176–184.
1227 Greenlund, A.C., Farrar, M.A., Viviano, B.L., and Schreiber, R.D. (1994). Ligand-induced
1228 IFN(γ) receptor tyrosine phosphorylation couples the receptor to its signal transduction system
1229 (p91). EMBO J. *13*, 1591–1600.
1230 Greenlund, A.C., Morales, M.O., Viviano, B.L., Yan, H., Krolewski, J., and Schreiber, R.D.
1231 (1995). Stat recruitment by tyrosine-phosphorylated cytokine receptors: An ordered reversible
1232 affinity-driven process. Immunity. *2*, 677–687.
1233 Gubser, C., Hué, S., Kellam, P., and Smith, G.L. (2004). Poxvirus genomes: A phylogenetic
1234 analysis. J. Gen. Virol. *85*, 105–117.
1235 Hagai, T., Azia, A., Babu, M.M., and Andino, R. (2014). Use of Host-like Peptide Motifs in
1236 Viral Proteins Is a Prevalent Strategy in Host-Virus Interactions. Cell Rep. *7*, 1729–1739.
1237 Hagmaier, K., Stock, N., Goodbourn, S., Wang, L.F., and Randall, R. (2006). A single amino
1238 acid substitution in the V protein of Nipah virus alters its ability to block interferon signalling
1239 in cells from different species. J. Gen. Virol. *87*, 3649–3653.
1240 Harrison, A.R., and Moseley, G.W. (2020). The Dynamic Interface of Viruses with STATs. J.
1241 Virol. *94*. e00856.
1242 Hauser, N., Gushiken, A.C., Narayanan, S., Kottilil, S., and Chua, J. V. (2021). Evolution of
1243 Nipah Virus Infection: Past, Present, and Future Considerations. Trop. Med. Infect. Dis. *6*, 24.
1244 Hernáez, B., Alonso-Lobo, J.M., Montanuy, I., Fischer, C., Sauer, S., Sigal, L., Sevilla, N., and
1245 Alcamí, A. (2018). A virus-encoded type I interferon decoy receptor enables evasion of host

immunity through cell-surface binding. Nat. Commun. *9*, 1–14.

Huang, J., Smirnov, S. V., Lewis-Antes, A., Balan, M., Li, W., Tang, S., Silke, G. V., Pütz, M.M., Smith, G.L., and Kotenko, S. V. (2007). Inhibition of type I and type III interferons by a secreted glycoprotein from Yaba-like disease virus. Proc. Natl. Acad. Sci. USA. *104*, 9822–9827.

Ihle, J.N. (2001). The Stat family in cytokine signaling. Curr. Opin. Cell Biol. *13*, 211–217.

Jensen, M.R., Yabukarski, F., Communie, G., Condamine, E., Mas, C., Volchkova, V., Tarbouriech, N., Bourhis, J.M., Volchkov, V., Blackledge, M., et al. (2020). Structural Description of the Nipah Virus Phosphoprotein and Its Interaction with STAT1. Biophys. J. *118*, 2470–2488.

Johnson, M., Zaretskaya, I., Raytselis, Y., Merezhuk, Y., McGinnis, S., and Madden, T.L. (2008). NCBI BLAST: a better web interface. Nucleic Acids Res. *36*, W5–W9.

Joklik, W.K. (1962). The purification of four strains of poxvirus. Virology. *18*, 9–18.

Kaneko, T., Huang, H., Zhao, B., Li, L., Liu, H., Voss, C.K., Wu, C., Schiller, M.R., and Li, S.S.C. (2010). Loops Govern SH2 Domain Specificity by Controlling Access to Binding Pockets. Sci. Signal. *3*, ra34.

Keiffer, T.R., Ciancanelli, M.J., Edwards, M.R., and Basler, C.F. (2020). Interactions of the Nipah Virus P, V, and W Proteins across the STAT Family of Transcription Factors. MSphere. *5*. e00449-20

Koksal, A.C., Nardozzi, J.D., and Cingolani, G. (2009). Dimeric Quaternary Structure of the Prototypical Dual Specificity Phosphatase VH1. J. Biol. Chem. *284*, 10129–10137.

Ladbury, J.E., and Arold, S.T. (2011). Energetics of Src Homology Domain Interactions in Receptor Tyrosine Kinase-Mediated Signaling. In Methods in Enzymology. *488*, 147–183.

Lasso, G., Honig, B., and Shapira, S.D. (2021). A Sweep of Earth's Virome Reveals Host-Guided Viral Protein Structural Mimicry and Points to Determinants of Human Disease. Cell

1271 Syst. *12*, 82-91.e3.

1272 Leung, S., Qureshi, S.A., Kerr, I.M., Darnell, J.E., and Stark, G.R. (1995). Role of STAT2 in
1273 the Alpha Interferon Signaling Pathway. Mol. Cell. Biol. *15*, 1312-1317

1274 Li, X., Leung, S., Kerr, I.M., and Stark, G.R. (1997). Functional subdomains of STAT2
1275 required for preassociation with the alpha interferon receptor and for signaling. Mol. Cell. Biol.
1276 *17*, 2048–2056.

1277 Liebschner, D., Afonine, P. V., Baker, M.L., Bunkoczi, G., Chen, V.B., Croll, T.I., Hintze, B.,
1278 Hung, L.W., Jain, S., McCoy, A.J., et al. (2019). Macromolecular structure determination using
1279 X-rays, neutrons and electrons: Recent developments in Phenix. Acta Crystallogr. Sect. D
1280 Struct. Biol. *75*, 861–877.

1281 Liu, R., Americo, J.L., Cotter, C.A., Earl, P.L., Erez, N., Peng, C., and Moss, B. (2021). One
1282 or two injections of MVA-vectored vaccine shields hACE2 transgenic mice from SARS-CoV-
1283 2 upper and lower respiratory tract infection. Proc. Natl. Acad. Sci. USA. *118*, e2026785118.

1284 Lu, Y., Stuart, J.H., Talbot-Cooper, C., Agrawal-Singh, S., Huntly, B., Smid, A.I., Snowden,
1285 J.S., Dupont, L., and Smith, G.L. (2019). Histone deacetylase 4 promotes type I interferon
1286 signaling, restricts DNA viruses, and is degraded via vaccinia virus protein C6. Proc. Natl.
1287 Acad. Sci. USA. *116*, 11997–12006.

1288 Ludlow, L.E., Lo, M.K., Rodriguez, J.J., Rota, P.A., and Horvath, C.M. (2008). Henipavirus
1289 V Protein Association with Polo-Like Kinase Reveals Functional Overlap with STAT1
1290 Binding and Interferon Evasion. J. Virol. *82*, 6259–6271.

1291 Mann, B.A., Huang, J.H., Li, P., Chang, H.C., Slee, R.B., O'Sullivan, A., Mathur, A., Yeh, N.,
1292 Klemsz, M.J., Brutkiewicz, R.R., et al. (2008). Vaccinia virus blocks Stat1-dependent and
1293 Stat1-independent gene expression induced by type I and type II interferons. J. Interf. Cytokine
1294 Res. *28*, 367–379.

1295 Mao, X., Ren, Z., Parker, G.N., Sondermann, H., Pastorello, M.A., Wang, W., McMurray, J.S.,

1296 Demeler, B., Darnell, J.E., and Chen, X. (2005). Structural bases of unphosphorylated STAT1
1297 association and receptor binding. Mol. Cell. *17*, 761–771.
1298 McWilliam, H., Li, W., Uludag, M., Squizzato, S., Park, Y.M., Buso, N., Cowley, A.P., and
1299 Lopez, R. (2013). Analysis Tool Web Services from the EMBL-EBI. Nucleic Acids Res. *41*.
1300 W597-W600
1301 Mendoza, J.L., Escalante, N.K., Jude, K.M., Sotolongo Bellon, J., Su, L., Horton, T.M.,
1302 Tsutsumi, N., Berardinelli, S.J., Haltiwanger, R.S., Piehler, J., et al. (2019). Structure of the
1303 IFNγ receptor complex guides design of biased agonists. Nature. *567*, 56–60.
1304 Miklossy, G., Hilliard, T.S., and Turkson, J. (2013). Therapeutic modulators of STAT
1305 signalling for human diseases. Nat. Rev. Drug Discov. *12*, 611–629.
1306 Mishra, P.M., Verma, N.C., Rao, C., Uversky, V.N., and Nandi, C.K. (2020). Intrinsically
1307 disordered proteins of viruses: Involvement in the mechanism of cell regulation and
1308 pathogenesis. In Progress in Molecular Biology and Translational Science. 174, 1–78.
1309 Montanuy, I., Alejo, A., and Alcami, A. (2011). Glycosaminoglycans mediate retention of the
1310 poxvirus type I interferon binding protein at the cell surface to locally block interferon antiviral
1311 responses. FASEB J. *25*, 1960–1971.
1312 Mossman, K., Upton, C., Buller, R.M.L., and McFadden, G. (1995). Species Specificity of
1313 Ectromelia Virus and Vaccinia Virus Interferon-γ Binding Proteins. Virology. *208*, 762–769.
1314 Malquer de Motes, C., Cooray, S., Ren, H., Almeida, G.M.F., McGourty, K., Bahar, M.W.,
1315 Stuart, D.I., Grimes, J.M., Graham, S.C., and Smith, G.L. (2011). Inhibition of apoptosis and
1316 NF-κB activation by vaccinia protein N1 occur via distinct binding surfaces and make different
1317 contributions to virulence. PLoS Pathog. *7*, e1002430.
1318 Malquer de Motes, C., Schiffner, T., Sumner, R.P., and Smith, G.L. (2014). Vaccinia virus
1319 virulence factor N1 can be ubiquitylated on multiple lysine residues. J. Gen. Virol. *95*, 2038–
1320 2049.

1321 Mühlemann, B., Vinner, L., Margaryan, A., Wilhelmson, H., de la Fuente Castro, C., Allentoft,
1322 M.E., de Barros Damgaard, P., Hansen, A.J., Holtsmark Nielsen, S., Strand, L.M., et al. (2020).
1323 Diverse variola virus (smallpox) strains were widespread in northern Europe in the Viking Age.
1324 Science. *369*, eaaw8977.
1325 Nagano, Y., Sugiyama, A., Kimoto, M., Wakahara, T., Noguchi, Y., Jiang, X., Saijo, S.,
1326 Shimizu, N., Yabuno, N., Yao, M., et al. (2020). The Measles Virus V Protein Binding Site to
1327 STAT2 Overlaps That of IRF9. J. Virol. *94*. e01169-20.
1328 Najarro, P., Traktman, P., and Lewis, J.A. (2001). Vaccinia Virus Blocks Gamma Interferon
1329 Signal Transduction: Viral VH1 Phosphatase Reverses Stat1 Activation. J. Virol. *75*, 3185–
1330 3196.
1331 Nguyen, K.B., Watford, W.T., Salomon, R., Hofmann, S.R., Pien, G.C., Morinobu, A., Gadina,
1332 M., O'Shea, J.J., and Biron, C.A. (2002). Critical role for STAT4 activation by type 1
1333 interferons in the interferon-γ response to viral infection. Science. *297*, 2063–2066.
1334 Oda, K., Matoba, Y., Irie, T., Kawabata, R., Fukushi, M., Sugiyama, M., and Sakaguchi, T.
1335 (2015). Structural Basis of the Inhibition of STAT1 Activity by Sendai Virus C Protein. J.
1336 Virol. *89*, 11487–11499.
1337 Park, E.M., Kang, J.H., Seo, J.S., Kim, G. Do, Chung, J., and Choi, T.J. (2008). Molecular
1338 cloning and expression analysis of the STAT1 gene from olive flounder, Paralichthys
1339 olivaceus. BMC Immunol. *9*, 1–9.
1340 Peters, N.E., Ferguson, B.J., Mazzon, M., Fahy, A.S., Krysztofinska, E., Arribas-Bosacoma,
1341 R., Pearl, L.H., Ren, H., and Smith, G.L. (2013). A Mechanism for the Inhibition of DNA-PK-
1342 Mediated DNA Sensing by a Virus. PLoS Pathog. *9*, e1003649.
1343 Qureshi, S.A., Leung, S., Kerr, I.M., Stark, G.R., and Darnell, J.E. (1996). Function of Stat2
1344 protein in transcriptional activation by alpha interferon. Mol. Cell. Biol. *16*, 288–293.
1345 Randall, R.E., and Goodbourn, S. (2008). Interferons and viruses: An interplay between

induction, signalling, antiviral responses and virus countermeasures. J. Gen. Virol. *89*, 1–47.

Rengachari, S., Groiss, S., Devos, J.M., Caron, E., Grandvaux, N., and Panne, D. (2018). Structural basis of STAT2 recognition by IRF9 reveals molecular insights into ISGF3 function. Proc. Natl. Acad. Sci. USA. *115*, E601–E609.

Robert, X., and Gouet, P. (2014). Deciphering key features in protein structures with the new ENDscript server. Nucleic Acids Res. *42*, W320–W324.

Rodriguez, J.J., Parisien, J.-P., and Horvath, C.M. (2002). Nipah virus V protein evades alpha and gamma interferons by preventing STAT1 and STAT2 activation and nuclear accumulation. J. Virol. *76*, 11476–11483.

Rodriguez, J.J., Cruz, C.D., and Horvath, C.M. (2004). Identification of the Nuclear Export Signal and STAT-Binding Domains of the Nipah Virus V Protein Reveals Mechanisms Underlying Interferon Evasion. J. Virol. *78*, 5358–5367.

Satterfield, B.A., Borisevich, V., Foster, S.L., Rodriguez, S.E., Cross, R.W., Fenton, K.A., Agans, K.N., Basler, C.F., Geisbert, T.W., and Mire, C.E. (2019). Antagonism of STAT1 by Nipah virus P gene products modulates disease course but not lethal outcome in the ferret model. Sci. Rep. *9*, 1–18.

Schindelin, J., Arganda-Carreras, I., Frise, E., Kaynig, V., Longair, M., Pietzsch, T., Preibisch, S., Rueden, C., Saalfeld, S., Schmid, B., et al. (2012). Fiji: An open-source platform for biological-image analysis. Nat. Methods. *9*, 676–682.

Schmidt, F.I., Bleck, C.K.E., Reh, L., Novy, K., Wollscheid, B., Helenius, A., Stahlberg, H., and Mercer, J. (2013). Vaccinia virus entry is followed by core activation and proteasome-mediated release of the immunomodulatory effector VH1 from lateral bodies. Cell Rep. *4*, 464–476.

Schneider, W.M., Chevillotte, M.D., and Rice, C.M. (2014). Interferon-stimulated genes: A complex web of host defenses. Annu. Rev. Immunol. *32*, 513–545.

1371 Shaw, M.L., García-Sastre, A., Palese, P., and Basler, C.F. (2004). Nipah Virus V and W
1372 Proteins Have a Common STAT1-Binding Domain yet Inhibit STAT1 Activation from the
1373 Cytoplasmic and Nuclear Compartments, Respectively. J. Virol. *78*, 5633–5641.
1374 Smart, O.S., Womack, T.O., Flensburg, C., Keller, P., Paciorek, W., Sharff, A., Vonrhein, C.,
1375 and Bricogne, G. (2012). Exploiting structure similarity in refinement: Automated NCS and
1376 target-structure restraints in BUSTER. Acta Crystallogr. Sect. D Biol. Crystallogr. *68*, 368–
1377 380.
1378 Smith, G.L., Benfield, C.T.O., Maluquer de Motes, C., Mazzon, M., Ember, S.W.J., Ferguson,
1379 B.J., and Sumner, R.P. (2013). Vaccinia virus immune evasion: Mechanisms, virulence and
1380 immunogenicity. J. Gen. Virol. *94*, 2367–2392.
1381 Smith, G.L., Talbot-Cooper, C., and Lu, Y. (2018). How Does Vaccinia Virus Interfere With
1382 Interferon? In Advances in Virus Research. *100*, 355–378.
1383 Soday, L., Lu, Y., Albarnaz, J.D., Davies, C.T.R., Antrobus, R., Smith, G.L., and Weekes, M.P.
1384 (2019). Quantitative Temporal Proteomic Analysis of Vaccinia Virus Infection Reveals
1385 Regulation of Histone Deacetylases by an Interferon Antagonist. Cell Rep. *27*, 1920-1933.e7.
1386 Stuart, J.H., Sumner, R.P., Lu, Y., Snowden, J.S., Smith, G.L., Muller, U., Steinhoff, U., Reis,
1387 L., Hemmi, S., Pavlovic, J., et al. (2016). Vaccinia Virus Protein C6 Inhibits Type I IFN
1388 Signalling in the Nucleus and Binds to the Transactivation Domain of STAT2. PLOS Pathog.
1389 *12*, e1005955.
1390 Symons, J.A., Alcamí, A., and Smith, G.L. (1995). Vaccinia virus encodes a soluble type I
1391 interferon receptor of novel structure and broad species soecificity. Cell. *81*, 551–560.
1392 Teo, H., Perisic, O., González, B., and Williams, R.L. (2004). ESCRT-II, an endosome-
1393 associated complex required for protein sorting: Crystal structure and interactions with
1394 ESCRT-III and membranes. Dev. Cell. *7*, 559–569.
1395 Torpey, N., Maher, S.E., Bothwell, A.L.M., and Pober, J.S. (2004). Interferon α but not

interleukin 12 activates STAT4 signaling in human vascular endothelial cells. J. Biol. Chem. *279*, 26789–26796.

Torres, A.A., Macilwee, S.L., Rashid, A., Cox, S.E., Albarnaz, J.D., Bonjardim, C.A., and Smith, G.L. Spir-1 promotes IRF3 activation and is targetted by vaccinia virus protein K7. BioRxiv. doi: 10.1101/2020.08.31.276659.

Unterholzner, L., Sumner, R.P., Baran, M., Ren, H., Mansur, D.S., Bourke, N.M., Randow, F., Smith, G.L., and Bowie, A.G. (2011). Vaccinia Virus Protein C6 Is a Virulence Factor that Binds TBK-1 Adaptor Proteins and Inhibits Activation of IRF3 and IRF7. PLoS Pathog. *7*, e1002247.

Vonrhein, C., Flensburg, C., Keller, P., Sharff, A., Smart, O., Paciorek, W., Womack, T., and Bricogne, G. (2011). Data processing and analysis with the autoPROC toolbox. Acta Crystallogr. Sect. D Biol. Crystallogr. *67*, 293–302.

Wang, B., Thurmond, S., Zhou, K., Sánchez-Aparicio, M.T., Fang, J., Lu, J., Gao, L., Ren, W., Cui, Y., Veit, E.C., et al. (2020). Structural basis for STAT2 suppression by flavivirus NS5. Nat. Struct. Mol. Biol. *27*, 875–885.

Wang, Y., Song, Q., Huang, W., Lin, Y., Wang, X., Wang, C., Willard, B., Zhao, C., Nan, J., Holvey-Bates, E., et al. (2021). A virus-induced conformational switch of STAT1-STAT2 dimers boosts antiviral defenses. Cell Res. *31*, 206–218.

Wennier, S.T., Brinkmann, K., Steinhäußer, C., Mayländer, N., Mnich, C., Wielert, U., Dirmeier, U., Hausmann, J., Chaplin, P., and Steigerwald, R. (2013). A Novel Naturally Occurring Tandem Promoter in Modified Vaccinia Virus Ankara Drives Very Early Gene Expression and Potent Immune Responses. PLoS One. *8*, e73511.

Wenta, N., Strauss, H., Meyer, S., and Vinkemeier, U. (2008). Tyrosine phosphorylation regulates the partitioning of STAT1 between different dimer conformations. Proc. Natl. Acad. Sci. USA. *105*, 9238–9243.

1421 Xue, B., Blocquel, D., Habchi, J., Uversky, A. V., Kurgan, L., Uversky, V.N., and Longhi, S.
1422 (2014). Structural disorder in viral proteins. Chem. Rev. *114*, 6880–6911.
1423 Yan, H., Krishnan, K., Greenlund, A.C., Gupta, S., Lim, J.T., Schreiber, R.D., Schindler, C.W.,
1424 and Krolewski, J.J. (1996). Phosphorylated interferon-alpha receptor 1 subunit (IFNaR1) acts
1425 as a docking site for the latent form of the 113 kDa STAT2 protein. EMBO J. *15*, 1064–1074.
1426 Yang, C., Mai, H., Peng, J., Zhou, B., Hou, J., and Jiang, D. (2020). STAT4: An
1427 immunoregulator contributing to diverse human diseases. Int. J. Biol. Sci. *16*, 1575–1585.
1428 Yang, Z., Cao, S., Martens, C.A., Porcella, S.F., Xie, Z., Ma, M., Shen, B., and Moss, B. (2015).
1429 Deciphering Poxvirus Gene Expression by RNA Sequencing and Ribosome Profiling. J. Virol.
1430 *89*, 6874–6886.
1431 Zhao, W., Lee, C., Piganis, R., Plumlee, C., de Weerd, N., Hertzog, P.J., and Schindler, C.
1432 (2008). A Conserved IFN-α Receptor Tyrosine Motif Directs the Biological Response to Type
1433 I IFNs. J. Immunol. *180*, 5483–5489.
1434